Journal of Structural Geology 33 (2011) 1105–1121

Contents lists available at ScienceDirect

Journal of Structural Geology

journal homepage: www.elsevier.com/locate/jsg

Strain softening along the MCT zone from the Sikkim Himalaya: Relative roles of Quartz and Micas

Kathakali Bhattacharyya*, Gautam Mitra

Department of Earth and Environmental Sciences, University of Rochester, Rochester, NY 14627, USA

ARTICLE INFO

Article history:
Received 13 July 2010
Received in revised form
2 March 2011
Accepted 8 March 2011
Available online 21 March 2011

Keywords:
Darjeeling - Sikkim Himalaya
Main Central thrust (MCT)
Mylonite zone
Strain softening
Type II fault zone

ABSTRACT

In the Darjeeling – Sikkim Himalaya, two distinct faults form the Main Central thrust (MCT), the structurally higher MCT1 and the lower MCT2; each has accommodated translation greater than 100 km. The lower MCT2 places Greater Himalayan amphibolite grade Paro-Lingtse gneiss over Lesser Himalayan greenschist grade Daling metapelites. The MCT2 is folded by the underlying Lesser Himalayan duplex and is exposed at different structural positions of the fold. At Pelling, the MCT2 zone is exposed as a ~373 m thick NW dipping fault zone that exposes ~19 m of hanging wall mylonitized Lingtse gneiss.

The Lingtse protolith shows evidence of amphibolite grade plastic deformation features in quartz and feldspar. Within the hanging wall mylonite zone (HWMZ), quartz and feldspar have undergone grain-size reduction by different deformation mechanisms and feldspars are sericitized suggesting the presence of fluids during deformation. We estimate a temperature of ~300 °C within the fault zone during fluid-assisted retrogression and deformation. Reaction softening of feldspars produced a large proportion of intrinsically weak matrix. This, in combination with development of a strong foliation defined by parallel mica grains, resulted in strain softening along the MCT2 zone, and concentrated the deformation along a thin zone or zones.

1. Introduction

The nature of deformation along major fault zones plays an important role in the overall mechanical evolution of mountain belts. The evolution of a fault zone or shear zone, under constant physical conditions, can be classified broadly into three main types: a Type I (Means, 1984) or strain hardening zone that thickens with increasing displacement (Hull, 1988; Mitra, 1992); a Type II (Means, 1984) or strain softening zone that localizes the deformation and can lead to a thin, and sometimes discrete, fault zone (Mitra, 1992); a Type III zone that maintains constant thickness throughout its history by balancing strain hardening and softening processes (Mitra, 1992). Any fault zone can evolve from one type to another with increasing displacement or changing physical conditions (Wojtal and Mitra, 1986), but most large displacement faults show softening characteristics at some stage during their deformation history.

Internal portions of fold-thrust belts (FTB) are generally characterized by dominant thrust sheets (Boyer and Elliott, 1982; Boyer and Geiser, 1987) that are carried by thrust faults with large translations along them (e.g. Elliott and Johnson, 1980; Boyer and Elliott, 1982; Butler and Coward, 1984; Gilotti and Kumpulainen, 1986; Srivastava and Mitra, 1994; McQuarrie and DeCelles, 2001). The fault rocks (Sibson, 1977) associated with such internal thrust sheets provide information on the strain softening mechanisms by which such large translations are accommodated along fault zones. During progressive evolution of any segment of a fault zone, strain softening can, for example, result from grain-size reduction leading to grain-size sensitive diffusional creep (e.g., Schmid, 1975; White et al., 1980; Mitra, 1984; Wojtal and Mitra, 1986; Gilotti, 1992; Srivastava and Mitra, 1996; Mitra and Ismat, 2001), reaction softening due to the development of a weak matrix from retrogressive breakdown of stronger phases (e.g. Mitra, 1978; Kerrich et al., 1980; Gilotti, 1992), geometric weakening due to parallel arrangement of weak planes of individual grains in a strongly foliated rock (e.g. Jordan, 1987), or low temperature changes in the presence of large volumes of fluid (e.g. Newman and Mitra, 1993, 1994). The relative importance of these various softening processes determines the overall behavior of the fault zone rocks. The mechanical evolution of any particular segment of a major fault zone depends on physical conditions (P, T, fluid pressure, displacement rate etc.) and lithology (composition, grain size) (Schmid, 1975; Sibson, 1977). Even for fault zones developed within a single lithology, such as quartzo-feldspathic continental crustal rocks, the actual deformation

* Corresponding author. Present address: Department of Earth System Sciences, Yonsei University, 134 Shinchon-Dong, Seodaemun-Gu, Seoul 120-749, Republic of Korea.
E-mail address: kathakali.bhattacharyya@gmail.com (K. Bhattacharyya).

0191-8141/$ – see front matter © 2011 Elsevier Ltd. All rights reserved.
doi:10.1016/j.jsg.2011.03.008

mechanisms can vary widely depending on physical conditions (e.g. Mitra, 1978, 1984, 1992; Wojtal and Mitra, 1988; Evans, 1991, 1993; Gilotti, 1992; Newman and Mitra, 1993; Srivastava and Mitra, 1996). In addition, the mechanisms can vary spatially along the length of a single fault as physical conditions change, such as when fault rocks are brought from deeper to shallower crustal conditions by progressive unroofing (Sibson et al., 1981; Wojtal and Mitra, 1988).

In the Himalayan FTB, the Main Central thrust (MCT) is a dominant north dipping thrust (Fig. 1) that carries a thick package of high grade ortho- and para-gneisses in its hanging wall, and extends along the entire 2500 km length of the Himalayan arc. The MCT zone was originally defined as the thrust fault that places the high grade Greater Himalayan sequence rocks southward over the lower grade Lesser Himalayan rocks (Heim and Gansser, 1939). Since then the position of the MCT has been a subject of great controversy. A large volume of existing work defines the nature and extent of the MCT fault zone on the basis of structural patterns (Mallet, 1875; Oldham, 1883; Heim and Gansser, 1939; Bordet et al., 1972; Le Fort, 1975; Pecher, 1975; Valdiya, 1980; Sinha-Roy, 1982; Gansser, 1983; Le Pichon et al., 1992; Srivastava and Mitra, 1996; Srivastava and Tripathy, 2007), change in metamorphic grade across the structural discontinuity (Parrish and Hodges, 1996; Daniel et al., 2003; Goscombe et al., 2006; Searle et al., 2008), and geochemical signatures (DeCelles et al., 1998, 2001, Robinson et al., 2001; Martin et al., 2005; Catlos et al., 2001, 2004). Regional balanced cross-sections constructed in different parts of the Himalayan FTB (Srivastava and Mitra, 1994; DeCelles et al., 2001; Robinson et al., 2006; McQuarrie et al., 2008) have shown that the MCT has displacements greater than 100 km along it.

Valdiya (1980) identified two different thrusts carrying the Greater Himalayan sequence of the Kumaon–Garhwal Himalaya, the structurally higher Vaikrita thrust and the structurally lower Munsiary thrust. In the Darjeeling – Sikkim Himalaya (Fig. 2), similar to the Kumaon–Garhwal Himalaya, we have identified two separate thrusts that form the MCT: the northern, structurally higher MCT1 and the southern, structurally lower MCT2 (Bhattacharyya and Mitra, 2009a; Mitra et al., 2010). The MCT2 zone is structurally equivalent to the North Almora/Munsiary thrust of the Kumaon–Garhwal Himalaya that has been studied in detail (Srivastava and Mitra, 1996).

In the Darjeeling – Sikkim Himalaya a regional balanced cross section (Mitra et al., 2010; Bhattacharyya, 2010) suggests that each of the MCT sheets has been translated for greater than 100 km and has brought crystalline rocks very close to the foreland; this is one of the largest translations from anywhere along the Himalayan arc. In order to understand the deformation mechanisms that accommodated such large translations we have studied in detail the microstructures and kinematic evolution of one of the fault zones, the MCT2 zone, that is well exposed near the town of Pelling in northwestern Sikkim (Fig. 2); our observations and conclusions are restricted to the MCT2 fault zone and do not apply to the MCT1 fault zone (Imamura et al., 2011) that lies farther to the north. The exposed fault at Pelling is a relatively thin zone where the hanging wall quartzo-feldspathic orthogneiss has undergone a prominent mineralogical change to form a quartz-mica mylonite (Bhattacharyya and Mitra, 2009b). In this paper, we address the question of how the mylonitization localized the large translation along a relatively thin fault zone at Pelling. In particular, we focus our attention on the relative importance of grain-size reduction by recrystallization and cataclasis, and the development of a weak foliated matrix by retrogressive reactions, in weakening the fault zone mylonites.

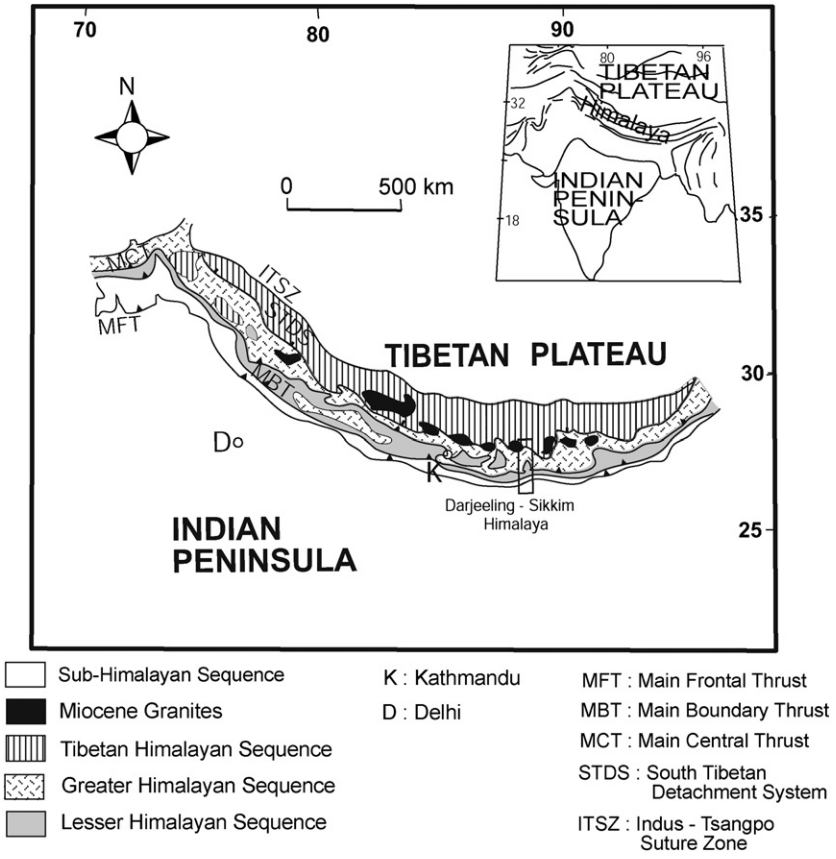

Fig. 1. Regional map of the Himalaya (Sorkhabi and Macfarlane, 1999) showing the major longitudinal lithotectonic subdivisions separated by major faults. In the Darjeeling-Sikkim Himalaya (rectangular outline), the MCT translates the hanging wall rocks of the Greater Himalayan sequence much farther southward than in the western Himalaya.

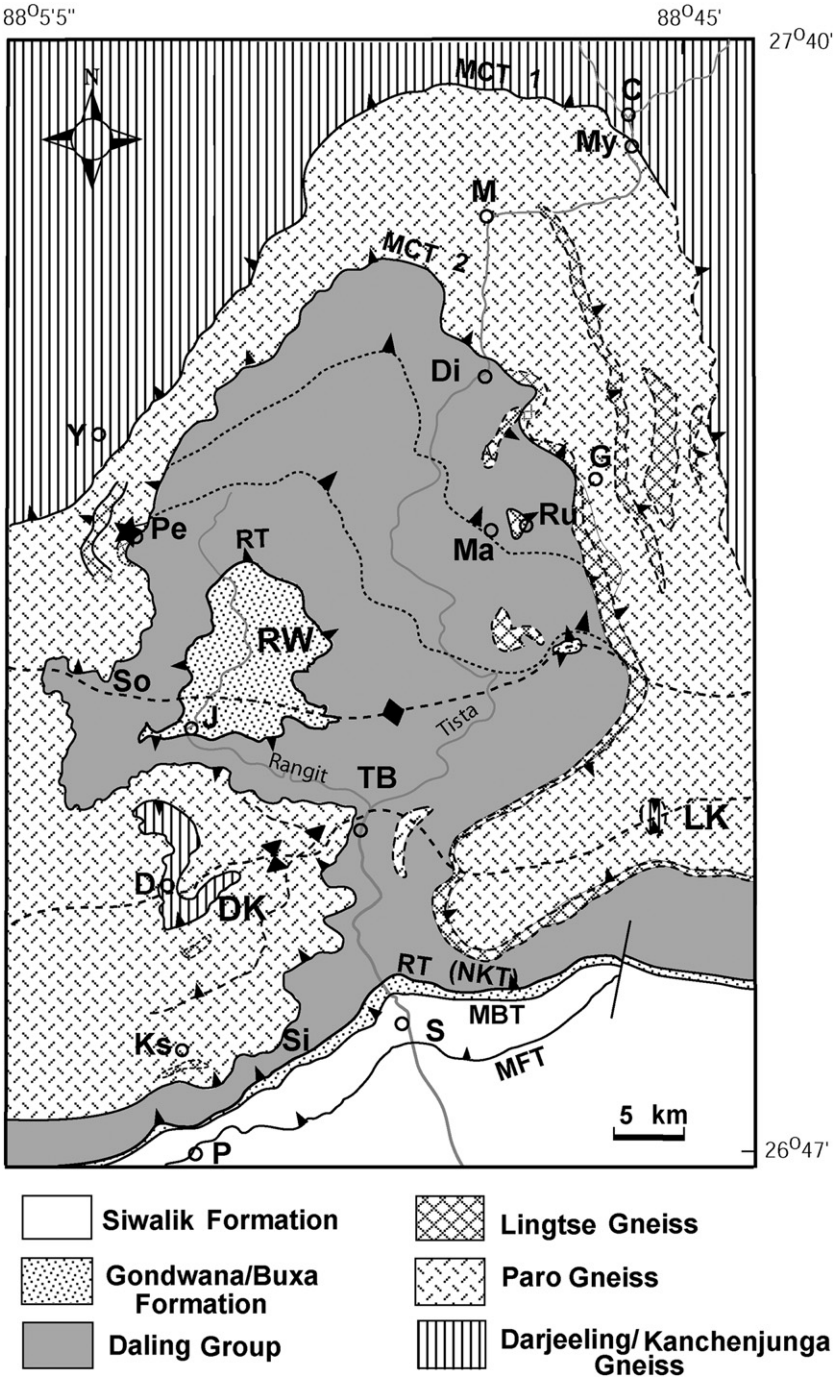

Fig. 2. Regional map of the Darjeeling – Sikkim Himalaya showing two separate thrust sheets, the MCT1 and MCT2, together forming the MCT. The Darjeeling/Kanchenjunga gneiss together with the Paro – Lintgse gneiss forms the Greater Himalaya sequence in this region. The MCT sheets are translated southward to within 5 km of the Himalayan mountain front and are exposed in the Darjeeling (DK) and the Labha (LK) semi-klippen. The folded MCT2 surround the Teesta half window and the fault zone is well exposed at Pelling (Pe). The main faults are labeled (see text for details). RW : Rangit window; towns shown are: C – Chungthang; D – Darjeeling; G – Gangtok; J – Jorethang; Ks – Kurseong; M – Mangan; P – Pankhabari; Pe – Pelling; S – Sevok; TB – Teesta Bazaar; Y – Yuksom.

Understanding the weakening processes is important not only for evaluating Himalayan tectonics, but has important implications for dominant thrusts in other mountain belts as well.

2. Regional geology

The Himalayan fold-thrust belt (FTB) formed as a result of collision between the Indian and Eurasian plates that initiated at ~52 Ma (Rowley, 1996) and is continuing to the present day. There are four major thrusts that have been identified all along the Himalayan arc: from north to south these are the Main Central thrust (MCT), the Ramgarh thrust (RT), the Main Boundary thrust (MBT) and the Main Frontal thrust (MFT). The MCT, MBT and MFT are traditionally well accepted (Medlicott, 1864; Heim and Gansser, 1939; Gansser, 1964), and the RT has been more recently described (Valdiya, 1980; Srivastava and Mitra, 1994; Pearson and DeCelles, 2005; Mitra et al., 2010). The MCT is the most internal of these Himalayan thrusts.

The Darjeeling-Sikkim Himalaya (Figs. 1 and 2, Mallet, 1875; Ray, 1947; Acharyya, 1971; Acharyya and Ray, 1977; Gangopadhyay and Ray, 1980; Schwan, 1980; Mukul, 2000; Bhattacharyya and Mitra, 2009a; Mitra et al., 2010) lies in the eastern Himalaya between longitudes 88°05′ E and 88°47'E, bounded by the Nepal Himalaya in the west and the Bhutan Himalaya in the east. The prominent Teesta half window (Schwan, 1980; Bhattacharyya and Mitra, 2009a; Mitra et al., 2010) exposes the greenschist facies metapelitic rocks of the Lesser Himalayan Sequence (LHS) with the high grade Greater Himalayan crystalline rocks exposed surrounding the half window. Similar to the Kumaon-Garhwal Himalaya (Valdiya, 1980; Srivastava and Mitra, 1994), we have identified two separate thrusts that carry the Greater Himalayan sequence (GHS) (Figs. 2 and 3, Mitra et al., 2010) in their hanging walls (HW). The northern thrust is the MCT1 that carries the granulite grade Kanchenjunga Gneiss in its hanging wall and places it on top of the amphibolite grade Paro group paragneisses and Lingtse orthogneisses. In northern Sikkim, the MCT1 zone is exposed as a ~1-km thick high grade mylonite zone (Imamura et al., 2011) that is equivalent to the Vaikrita thrust zone of the Kumaon-Garhwal Himalaya (Valdiya, 1980; Srivastava and Mitra, 1994). The southern thrust, the MCT2, carries the Paro-Lingtse gneisses in its HW and places them over the greenschist grade Daling sequence of the LHS. The MCT2 zone is exposed as a greenschist grade mylonite zone in the Darjeeling – Sikkim Himalaya and is equivalent to the Munsiary thrust and the North and South-Almora thrusts of the Kumaon-Garhwal Himalaya (Valdiya, 1980; Srivastava and Mitra, 1994). The regional structure of the Darjeeling – Sikkim Himalaya suggests that the MCT sheets were folded by the growth of the underlying Lesser Himalayan duplex (Fig. 3, Bhattacharyya and Mitra, 2009a; Mitra et al., 2010) into a regional antiform–synform pair and were translated southward as part of the duplex roof sequence; these rocks (i.e., the MCT sheets)

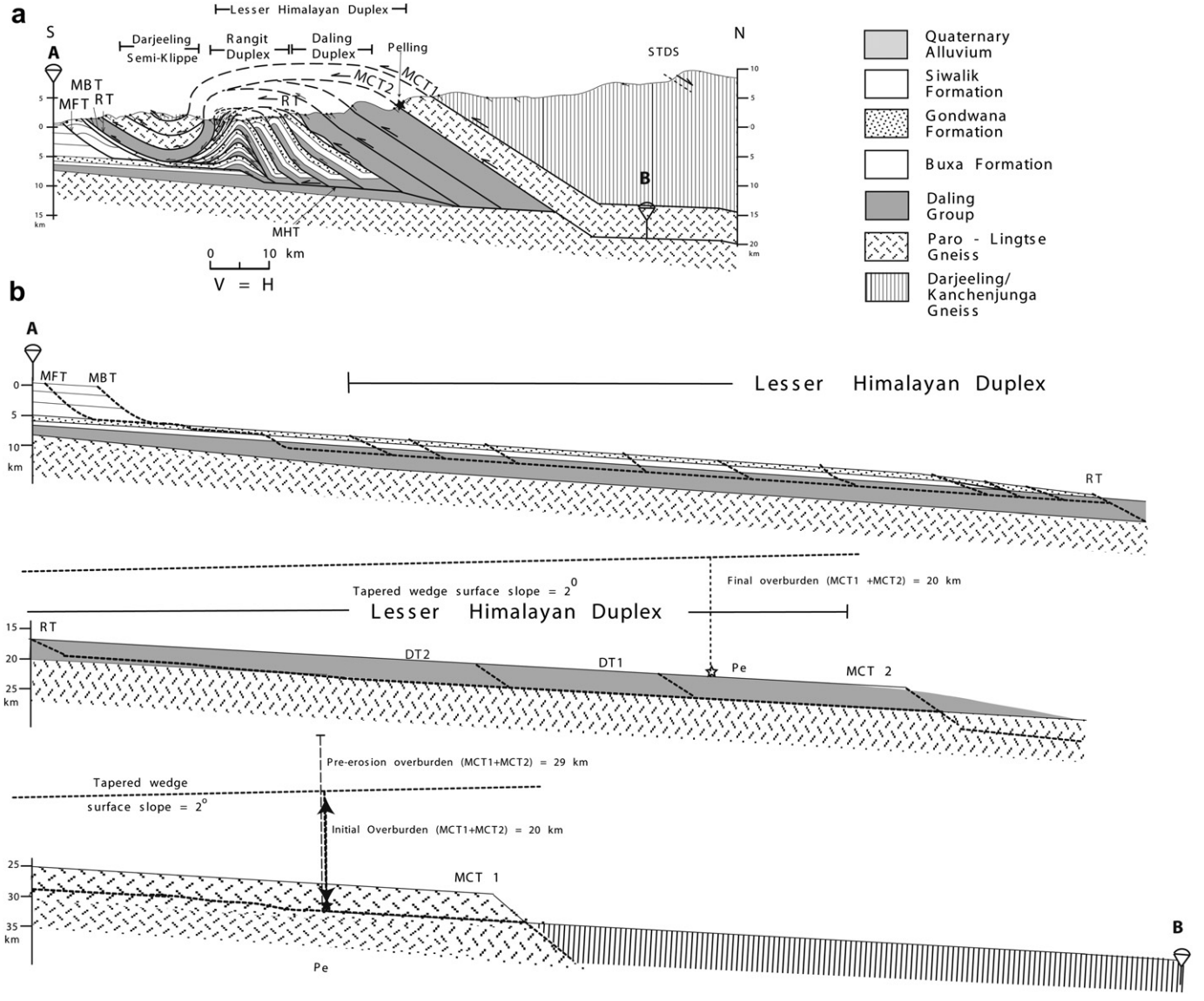

Fig. 3. (a) Regional balanced cross-section of the Darjeeling – Sikkim Himalaya showing the structurally higher MCT1 and lower MCT2 sheets, both folded by the growth of the Lesser Himalayan duplex into a regional antiform-synform pair. The location of the Pelling MCT2 mylonite zone in the northern limb of the regional antiform is shown on the deformed cross section. (b) Restored cross section shows that each of the MCT sheet has undergone ~100 km translation in the Darjeeling – Sikkim Himalaya. The position of the undeformed protolith of the Pelling MCT2 mylonite zone is shown with a filled star on the restored section; the location of the fault zone at the end stages of deformation is shown in the footwall with an open star. The surface slope of the tapered crystalline orogenic wedge is shown with a dashed line (Huyghe et al., 2001). Based on the balanced cross section and effects of erosion, an overburden of ~20 km is estimated for the protolith at the initiation of movement on the MCT2. The pre-erosion overburden is estimated as ~29 km (see text for details). Metamorphic mineral assemblage (see text for details) was used to confirm depth estimates.

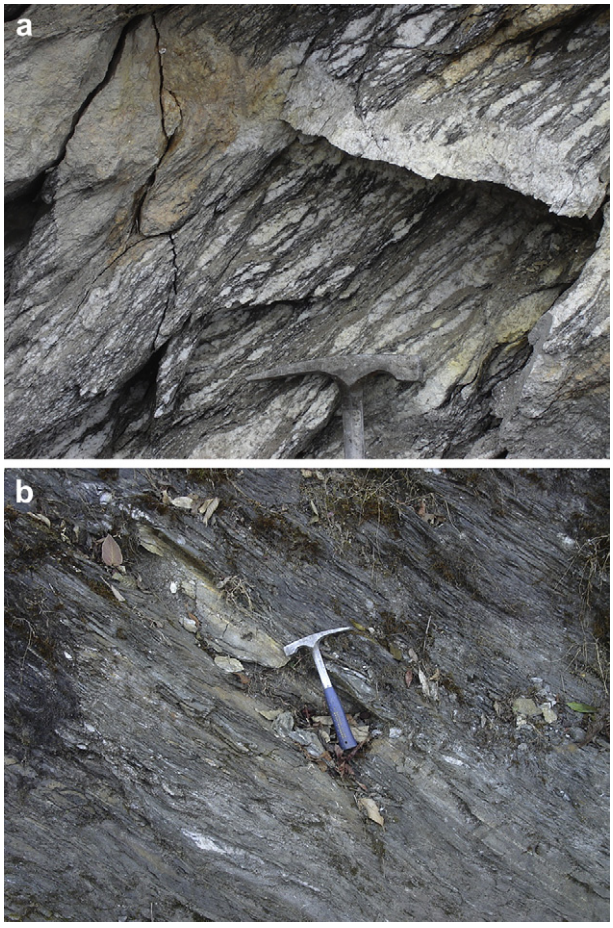

Fig. 4. (a) Hanging wall Lingtse gneiss protolith lying immediately outside the MCT2 zone. It is an amphibolite grade, coarse grained, biotite-muscovite-bearing quartzo-feldspathic orthogneiss that contains feldspar augen; hammer head for scale. (b) Chlorite bearing greenschist grade, Daling phyllites from immediately outside the MCT2 zone that form the footwall rocks; hammer for scale.

are exposed in the synformal core of the Darjeeling klippe. The window-klippe outcrop patterns suggest a minimum displacement of ~80 km and based on our balanced cross-section (Fig. 3, Mitra et al., 2010) we estimate that the MCT sheets have each undergone displacements of more than 100 km. Both MCT zones are exposed at different structural positions on the regional antiform–synform pair. In this paper, we focus our attention on the MCT2 zone from the northern limb of the regional antiform that is exposed in the northwestern part of the Teesta window near the town of Pelling in West Sikkim (Fig. 3, Bhattacharyya and Mitra, 2009b).

3. Pelling mylonite zone

At Pelling, the MCT2 zone is exposed as a northwesterly dipping greenschist grade mylonite zone, with an average attitude of 43°, 305° (Bhattacharyya and Mitra, 2009b). The hanging wall rocks are the Greater Himalayan amphibolite grade quartzo-feldspathic Lingtse gneiss (Fig. 4a); the footwall rocks are the Lesser Himalayan greenschist grade chlorite schists and slates of the Daling Group (Fig. 4b). Immediately west of Pelling town-square, the deformed hanging wall Lingtse gneiss is exposed as a ~32-m wide northwesterly dipping mylonite zone along a traverse that trends 95°–275°. The average apparent dip of the exposed mylonitic foliation along the traverse is ~39°, giving an apparent thickness of the exposed hanging wall mylonite zone (HWMZ) of ~20 m (Fig. 5). The true thickness of the exposed HWMZ is ~19 m. Along the traverse line the hanging wall protolith is exposed ~100 m NW of the exposed HWMZ, while the closest footwall protolith is exposed ~500 SE of the HWMZ. Thus, the maximum thickness of the MCT2 zone at Pelling is ~373 m.

Within the HWMZ, there is progressive grain-size reduction and change in composition from a quartzo-feldspathic gneiss (protolith) to a quartz-mica mylonite. We have subdivided the HWMZ into three different domains based on the grain size, and matrix and prophyroclast percentages. Along the exposed traverse, the uppermost part of the exposed HWMZ is a ~7.7 m thick protomylonite zone. Below this lies a ~8.3 m thick zone of mylonite. The lowest part of the exposed HWMZ, closest to the footwall contact, is made up of ~4 m thick zone of strongly deformed mylonite that has some thin bands of ultramylonite within it. Because these thicknesses are measured in a direction of apparent dip they are apparent thicknesses; the true thicknesses of these three zones are estimated to be ~7 m, ~8 m and ~4 m respectively. Here, we describe the microstructural and mineralogical changes of the protolith in the ~19 m thick mylonite zone.

3.1. Microstructures

3.1.1. Protolith

The Lingtse gneiss is a coarse-grained biotite-muscovite-bearing quartzo-feldspathic orthogneiss (Figs. 4a and 6a) that has a pre-Himalayan gneissic foliation with leucocratic quartz-feldspar layers alternating with darker mafic layers. Modal percentages based on point-count data show that the rock is made up of quartz (~40%), feldspar (~25%), biotite (~28%) and muscovite (~6%) (Fig. 7); in other words, feldspar grains are a major constituent of the protolith. The orthogneiss preserves some primary igneous textures, including poikilitic, graphic and myrmekitic textures (Fig. 6a), that have survived the pre-Himalayan metamorphism.

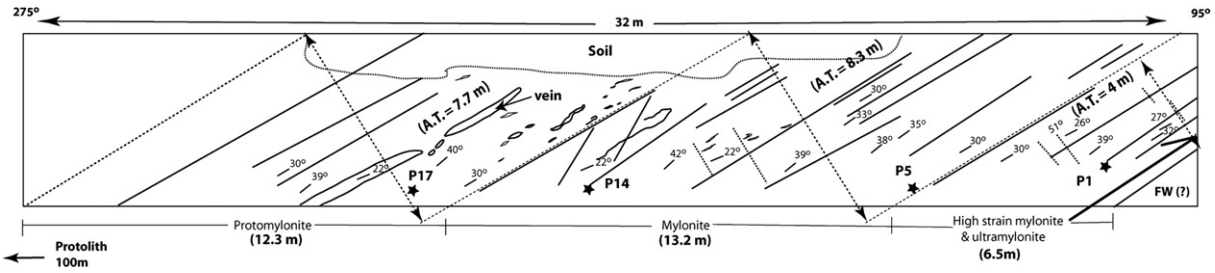

Fig. 5. Outcrop sketch of the ~32 m wide MCT2 mylonite zone outcrop that exposes the deformed Lingtse gneiss protolith near Pelling along a traverse that trends 95°–275°. The average attitude of the mylonite zone is 43°, 305°. The undeformed protolith lies ~100-m northwest of the exposed hanging wall mylonite zone (HWMZ). We have subdivided the HWMZ into three different domains based on the grain size, and matrix and prophyroclast percentages. The dashed lines mark the boundaries between the three sub-zones, namely the protomylonite zone (~7.7 m thick), the mylonite zone (~8.3 m thick) and the high strain mylonite zone (~4 m thick); the apparent thickness of the HWMZ along the traverse is estimated to be ~20 m. The true thickness of the HWMZ is ~19 m. The locations of the samples analyzed for this study are shown in stars. A.T. – Apparent thickness, FW – Footwall.

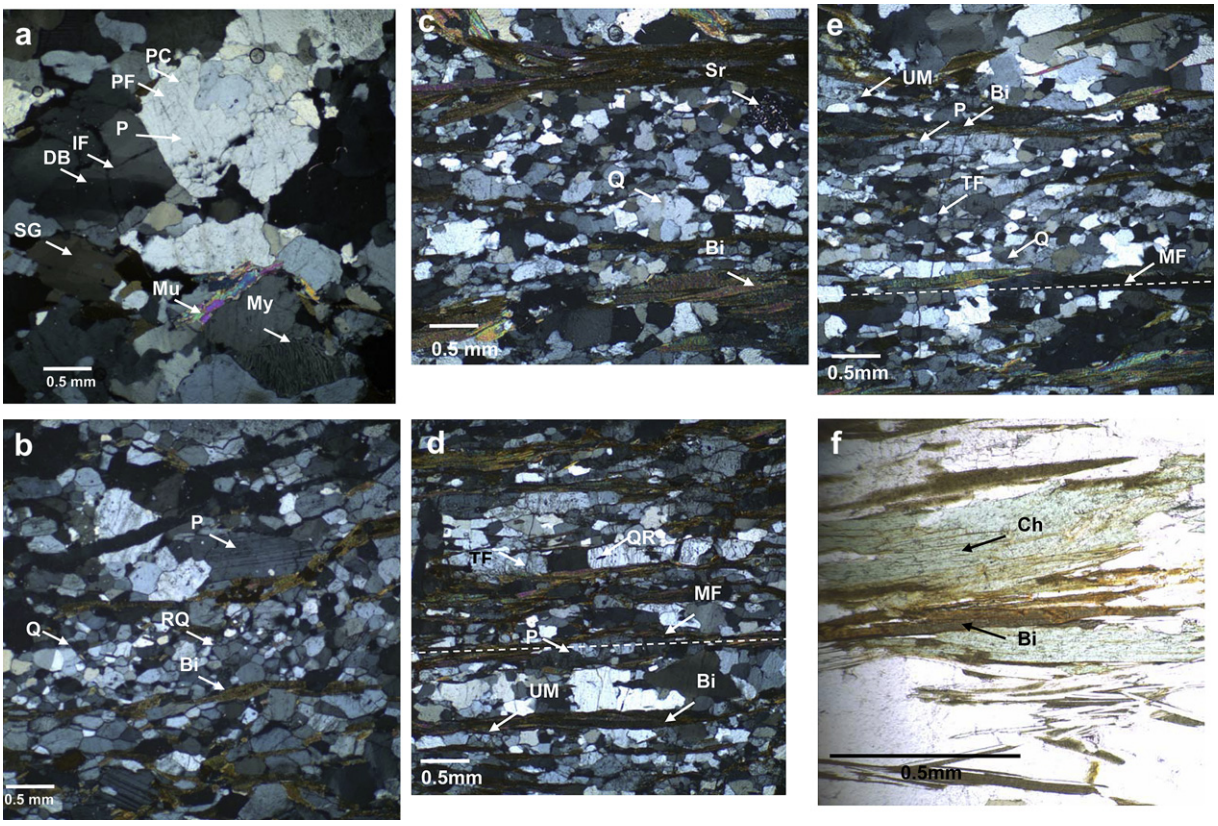

Fig. 6. (a) Photomicrograph, under crossed nicols, of the coarse grained, muscovite (Mu)- biotite – quartzo (Q) – feldspathic (P) Lingtse gneiss protolith. Quartz grains show subgrain formation (SG), deformation bands (DB), and dislocation controlled intragranular fracturing (IF). Plagioclase feldspar grains (P) show intragranular fracturing (PF) mostly parallel to the crystallographic cleavage planes (PC). The protolith also preserves remnant igneous, myrmekitic (My) texture. (b) Photomicrograph of the protomylonite (sample number P17) showing a prominent grain-size reduction in quartz by recrystallization and subgrain formation that form the matrix (RQ). Compared to the protolith, there is a pronounced development of a mylonitic foliation defined by the recrystallized quartz grains and biotites (Bi). Plagioclase feldspars (P) also show grain-size reduction dominantly by fracturing. (c) Photomicrograph, under crossed nicols, of the mylonite (sample number P14) that shows an increase in the proportion of matrix, defined by recrystallized quartz (Q) and micas (e.g., biotite, Bi). Quartz porphyroclasts are present (Q) that show core-mantle structure. Feldspars show evidence of sericitization (Sr). (d) Photomicrograph of the mylonite from farther toward the base of the mylonite zone (sample number P5); there is an increase in the proportion of mucovite, biotite (Bi) and chlorite that segregate into different layers that alternate with quartz-rich layers forming a strong mylonitic foliation (MF). There are a few ribbon quartz grains present (QR) and also a few plagioclase feldspar grains (P); late transgranular fractures (TF) can be seen that cross cut the mylonitic foliation. (e) Photomicrograph from the high strain mylonite zone (sample number P1) showing thin bands of ultramylonite (UM) mostly defined by recrytallized quartz grains; late transgranular fractures (TF) are most prominent in this thin section. (f) Photomicrograph, under plane polarized light, from the high strain mylonite zone shows the largest amount of retrogression of biotite (Bi) to chlorite (Ch).

Undulose extinction is the most dominant microstructure in quartz, followed by subgrain formation and deformation bands (Fig. 6a). Some of the quartz grains also show intragranular fracturing and a few quartz grains show transgranular fracturing.

We carried out point-count analysis of deformation microstructures along eight equally spaced parallel transects (Sussman, 1995), using a semi-automatic counting stage. The observed microstructures, as seen in the different minerals, are expressed as the percentage of total number of grains of each mineral. The results (Fig. 8a) show that ~36% of all quartz grains show undulose extinction; subgrain formation is the second dominant structure and is seen in ~29.5% of quartz grains. Deformation bands are seen

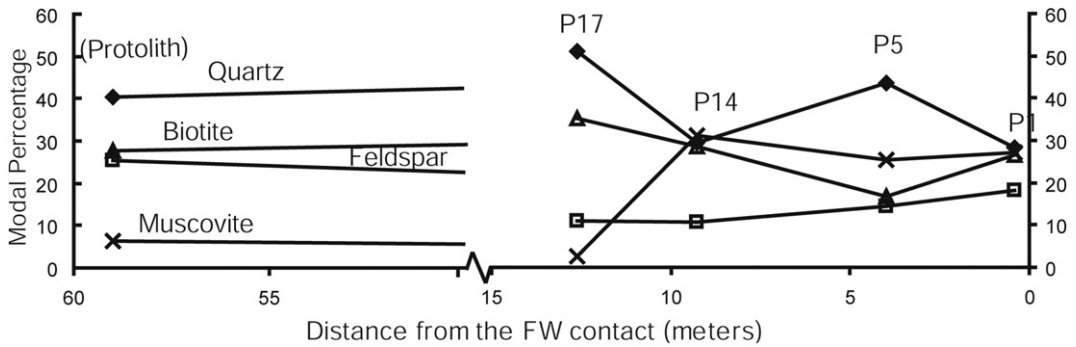

Fig. 7. Variation of the modal percentages of quartz, feldspar, biotite and muscovite grains with distance from the footwall contact. Note the inverse relationship between feldspars and quartz + muscovite suggesting sericitization or reaction softening of feldspars, in the presence of fluids. The sample numbers are shown in the figure; locations of the fault zone samples are shown in Fig. 5.

in ~6.5% of the quartz grains, while intragranular and transgranular fractures are seen in ~24.5% and ~3.5% of the quartz grains respectively. The intragranular fractures in quartz generally form in three directions originating from opaque mineral inclusions or grain-to-grain contacts. The very few transgranular fractures that are present in the quartz grains are at high angles to the tectonic foliation in the rock.

Plagioclase is the dominant feldspar in the Lingste gneiss protolith making up ~80% of the total feldspar percentage, with alkali feldspars making up the remaining ~20%. Both types of feldspar grains show microstructures like deformation bands, deformation twins, continuous, sweeping undulose extinction, and subgrain formation. The feldspars also show evidence of considerable intragranular and transgranular fracturing (Fig. 6a).

Results from point-count analysis (Fig. 8a) reveal that feldspar grains have almost equal proportions of grains showing undulose extinction (~15%), subgrain formation (~15%), deformation bands (~15%), and deformation twins (~15%). The percentages of feldspar grains with intragranular and transgranular fracturing are ~38% and ~15% respectively. It is interesting to note here that some feldspar grains show zones of patchy undulose extinction that are closely associated with the fractures.

3.1.2. Protomylonite zone

As described earlier the protomylonite zone lies closest to the protolith (Fig. 5), and is ~7 m thick. The rock is more strongly deformed than the protolith and is made up of quartz, plagioclase feldspars, alkali feldspars, muscovite, biotite, chlorite and epidote. Here the muscovites, biotites and a few chlorite grains form the phyllosilicate component that define the mylonitic foliation; ~0.2 mm thick bands of phyllosilicates alternate with ~0.5–1.0 mm thick bands primarily made up of fine-grained quartz matrix and coarser plagioclase (Fig. 6b). There is an increase in the modal percentage of quartz grains (~50%) compared to the protolith, and a decrease in the proportion of feldspar grains (~11%) (Fig. 7).

There are two broad grain size groups observed within the quartz grains. The relatively coarser quartz grains (>50 μm) are porphyroclasts of original quartz grains; they show strong undulose extinction. The finer grains (<30 μm) are generally equant in shape and have slightly wavy to straight grain boundaries forming triple junctions (Fig. 6b); these grains also show undulose extinction. There are a few intragranular fractures, mostly radiating from inclusions within grains, and some grains also show some transgranular fractures.

The relative proportions of the different microstructures seen in the quartz grains are shown in Fig. 8b; they include subgrain formation in ~46% of all quartz grains, followed by undulose extinction (~42% of grains), deformation bands (~0.5%), intragranular fracturing (~5%), and transgranular fracturing (~4.8%).

Feldspar grains show evidence of late intragranular and transgranular fractures that overprint the earlier microstructures such as continuous undulose extinction and deformation twinning (Fig. 6b). Smaller feldspar grains that are < 30 μm, also show evidence for subgrain formation. There are a few (~16%) finer plagioclase grains (~15 μm) that constitute the fine-grained matrix along with the finer quartz grains (<20 μm). These fine plagioclase grains are generally equant in shape and form triple junctions. The coarser feldspar grains show both sweeping, continuous undulose extinction and patchy undulose extinction that are closely associated with fractures. Coarser feldspar grains have been fractured with the fracture planes generally being parallel to the crystallographic cleavage planes. The feldspar grains also show alteration to quartz and muscovite (sericitization) and epidote and muscovite (saussiritization).

The point-count results of the different microstructures within feldspar grains are summarized in Fig. 8b; intragranular and transgranular fractures are seen in ~32% of all the feldspar grains, followed by undulose extinction in ~33% of feldspar grains and subgrain formation in ~4% of the feldspar grains. Therefore, compared to the protolith (Fig. 8a), where ~53% of feldspar grains show fractures, in the protomylonite zone there are more feldspar grains (~64%) showing evidence of fracturing that overprint the earlier microstructures.

The muscovite grains show two different types of spatial associations. The finer muscovite grains (<20 μm) are, in general, spatially associated with the feldspar grains, while the coarser grains are associated with the biotite and chlorite grains, and together they define the mylonitic foliation. Some of the biotite grains are intergrown with chlorite grains and the boundaries between the two minerals are indistinct.

3.1.3. Mylonite zone

As described earlier the mylonite zone lies below the protomylonite zone and its base is ~6.5 m from the footwall contact along the line of travesrse (Fig. 5). The mylonite zone is estimated to be ~8 m thick, and the mylonite is made up of quartz, muscovite, biotite, plagioclase, chlorite and epidote. Mineralogically this is similar to the protomylonite zone, although there is an increase in the proportion of matrix (with grain size < 20 μm) as defined by the fine-grained quartz and phyllosilicate minerals (Fig. 6c, d). The mylonitic foliation is defined by elongated quartz augen, ribbon quartz, some feldspar augen and micas (Fig. 6d). In this zone, there is a prominent segregation of ~0.3 mm thick phyllosilicate mineral bands that alternate with ~0.5 mm thick dominantly quartz-rich bands (Fig. 6d). The segregation into bands becomes more prominent toward the base of the mylonite zone. There is a further reduction in the proportion of feldspars in this zone (~10%). Quartz, along with a few remaining plagioclase feldspars, are the two dominant porphyroclasts (Fig. 6c).

The fine-grained quartz grains that form the matrix, continue to show undulose extinction. There are quartz porphyroclasts present in this zone that are ~1.0–1.5 mm in diameter (Fig. 6c) and some of these porphyroclasts are asymmetric (σ-type) with top-to-the-SE shear sense. These prophyroclasts have very fine-grained outer parts and coarser subgrains in the bulbous cores forming core-mantle structure. There is also an abundance of ribbon quartz (~1.0–1.5 mm) in this zone (Fig. 6d). The quartz grains also show some intragranular and transgranular fractures.

The relative proportions of different microstructures as seen in the quartz grains of all kinds (coarse and fine) is shown in Fig. 8c, d. Undulose extinction is seen in ~49% of all quartz grains, followed by subgrain formation in ~33% of quartz grains, core-mantle structures (~2%), deformation bands (~0.3%), intragranular fractures (~10%) and transgranular fractures (~5%). Compared to the protomylonite zone, there is an increase in the proportion of quartz grains showing undulose extinction from ~42%–~49% and a decrease in the proportion of quartz grains showing subgrain formation from ~46%–~33% within the mylonite zone.

The remaining feldspars are mainly plagioclase and form porphyroclasts. Fracturing is the most dominant microstructure seen in the feldspars within this zone; the intragranular fractures are generally parallel to the mineral cleavage planes (Fig. 6c), and there are also a few conjugate fractures. Some of the feldspar grains show patchy undulose extinction. Sericitization (Fig. 6c) is more prominent in this zone than in the protomylonite zone.

The relative proportions of the different microstructures seen in the feldspar grains (Fig. 8c, d) are undulose extinction (~23% of grains), intragranular fractures (~51% of grains), and transgranular fractures (~25% of grains). Hence, there is a progressive increase in

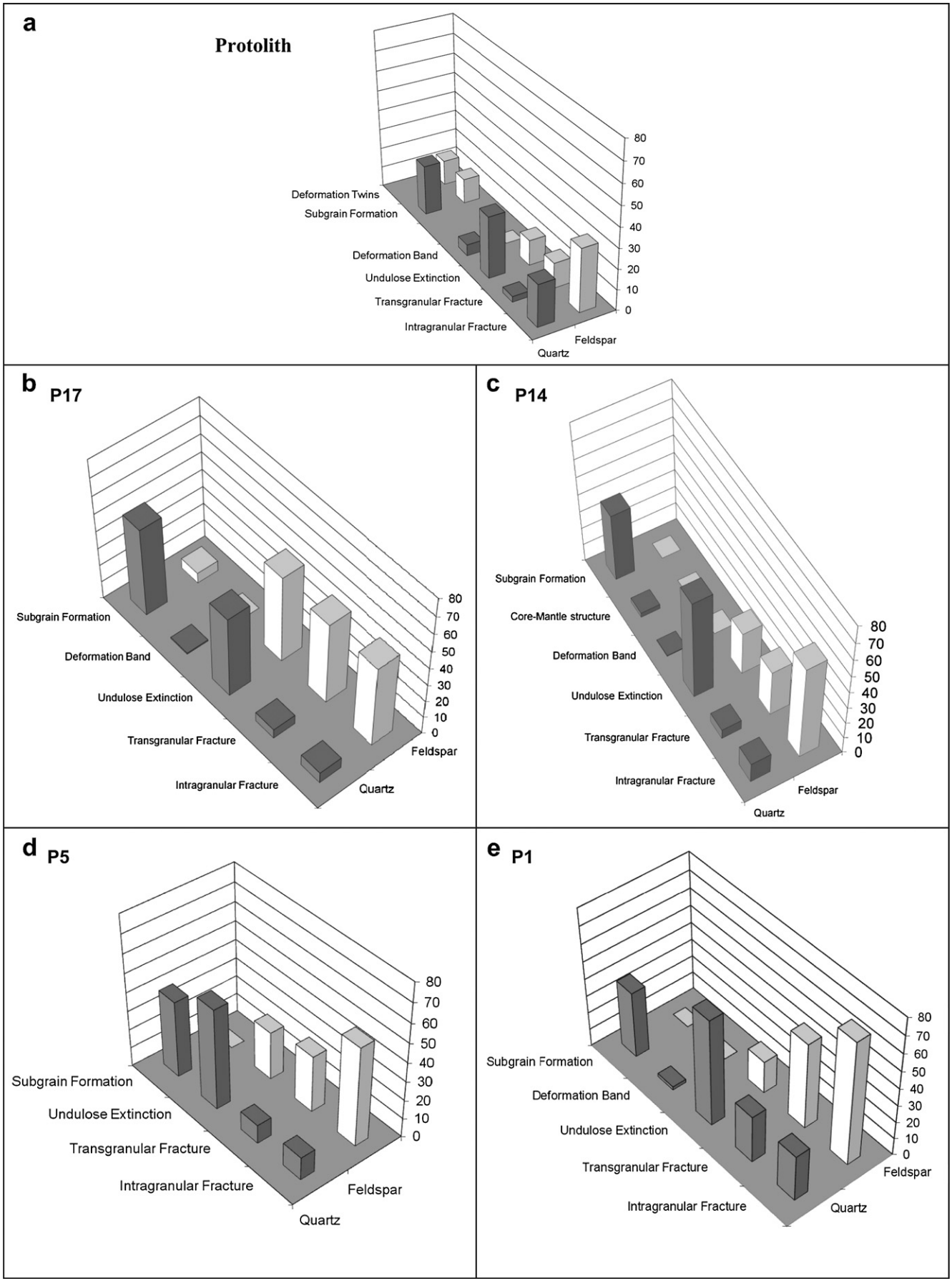
a
Protolith
Deformation Twins
Subgrain Formation
Deformation Band
Undulose Extinction
Transgranular Fracture
Intragranular Fracture
Feldspar
Quartz
80
70
60
50
40
30
20
10
0
b
P17
Subgrain Formation
Deformation Band
Undulose Extinction
Transgranular Fracture
Intragranular Fracture
Feldspar
Quartz
c
P14
Subgrain Formation
Core-Mantle structure
Deformation Band
Undulose Extinction
Transgranular Fracture
Intragranular Fracture
Feldspar
Quartz
d
P5
Subgrain Formation
Undulose Extinction
Transgranular Fracture
Intragranular Fracture
Feldspar
Quartz
e
P1
Subgrain Formation
Deformation Band
Undulose Extinction
Transgranular Fracture
Intragranular Fracture
Feldspar
Quartz

the proportion of fracturing in the feldspar grains from the protolith through the protomylonite zone to the mylonite zone.

The proportions of the phyllosilicate minerals in this zone are higher than in the protomylonite zone, but the mineralogical components are the same in the two zones. There is a prominent increase in the proportion of muscovite grains, from ~5% in the protomylonites to ~28% within the mylonites; these phyllosilicates segregate into layers forming the mylonitic foliation (Fig. 6d).

3.1.4. High strain mylonites with ultramylonite bands

The high strain mylonites, as described earlier, are exposed in a zone whose true thickness is estimated to be ~4 m. There are no prophyroclasts present within the zone and there are ~2 mm thick bands of ultramylonites (Fig. 6e), dominantly defined by very fine-grained quartz grains (<15 μm) and a few remaining plagioclase feldspar grains. In this zone, the mylonitic foliation is mainly defined by the phyllosilicates, and the thin bands of ultramylonites run parallel to the foliation. The mineral assemblage is similar to that in the protomylonite and mylonite zones with ~29% of quartz and ~18% of feldspar grains, but the modal percentages of the phyllosilicates is the highest in this zone (~55%; Fig. 7). This change in composition has important implications for the mechanical behavior of the MCT2 zone as described later (Section 5).

Fine-grained quartz predominantly forms the matrix and there are no identifiable quartz prophyroclasts present; the quartz grains continue to show undulose extinction. Quartz grains also show transgranular fractures that cross cut the mylonitic foliation (Fig. 6e). Results from point-count analysis (Fig. 8e) show the relative proportions of different microstructures seen in quartz grains; these are undulose extinction (~40% of grains), subgrain formation (~25%), deformation bands (~1%), intragranular fractures (~17%), and transgranular fractures (~18%). Thus, there is an increase in the proportion of quartz grains showing fracturing compared to quartz grains in the protomylonites and mylonites.

Plagioclase is the dominant feldspar in this zone. Fracturing in feldspars is the dominant microstructure, and it overprints earlier microstructures. Sericitization of feldspars is also most prominent in this zone. We interpret this direct relationship between fracturing and sericitization of feldspars to be a key factor in controlling the deformation within the MCT2 zone (Section 5). Results from the point-count analysis (Fig. 8e) show the relative proportions of the different microstructures recorded in feldspar grains: grains showing intragranular fractures (seen in ~51% of feldspar grains) and transgranular fractures (~35% of grains) dominate over feldspar grains showing subgrain formation (~14% of grains). Thus, within the exposed part of the HWMZ, fracturing in feldspars progressively increases toward the base of the mylonite zone.

Muscovite, chlorite and biotite are the phyllosilicate in this zone. The brown colored biotites are intergrown with green colored chlorites as seen under plane polarized light and the boundaries between the two minerals are indistinct (Fig. 6f). This relationship is most strongly developed in this zone.

3.2. Grain size data

Grain size distribution within a mylonite zone plays a critical role in determining the dominant deformation mechanisms within the zone. We have carried out Spektor chord analysis on the HWMZ samples using a linear integrating stage. The method assumes that each rock is made up of a polydispersed system of spherical grains (Underwood, 1970; Mitra, 1978). Thin sections from the rock samples were studied along four transects that are 0°, 45°, 90° and 135° to the foliation. We measured the chord lengths of different grains along these transects and subdivided the chord lengths into classes with a class interval of 15 μm. For every size-class, we determined the number of chords per unit length of the test line, and used this quantity to calculate the number of particles per unit volume in that size-class (Underwood, 1970; Mitra, 1978). Thus, we obtained the grain size distributions of quartz, plagioclase feldspars, muscovite and biotite within the HWMZ (Fig. 9).

The Lingtse gneiss protolith shows a spread in the frequency distribution of grain sizes for all four major mineral constituents, namely, quartz, feldspar, muscovite and biotite (Fig. 9a). The coarsest grain-size peak for quartz is at ~140 μm while the finest is at ~38 μm; the geometric mean grain size for quartz is ~86 μm. The finest quartz grain size (~28 μm) is associated with the primary poikilitic texture of the orthogneiss. The feldspars are also coarse grained with a prominent peak at ~116 μm and the coarsest grains (~290 μm) are phenocrysts; the geometric mean grain size of feldspar is ~135 μm. The muscovite and the biotite grains show a broad range of grain sizes with the highest frequencies at ~35 μm and ~24 μm respectively. The geometric mean grain sizes of muscovite and biotite are ~52 and ~51 μm respectively.

Within the protomylonite, there are two prominent frequency peaks for quartz grains at ~52 μm and ~15 μm; the coarser grain size represents the porphyroclasts of the original quartz grains and the finer grain size corresponds to the matrix. Thus, there is a distinct grain-size reduction in quartz (Fig. 9b) as compared to the protolith. The highest frequency peak for feldspar grains is at ~36 μm (Fig. 9b) with a smaller peak at ~15 μm. The finer feldspar grains peak represents the matrix. Thus, both quartz and feldspar grains show significant grain-size reduction from the protolith to the protomylonite (Fig. 9a, b). Compared to the protolith, both muscovites and biotites also show a finer grain size (15–30 μm) in the protomylonite zone.

The mylonite zone shows an overall similar spread in the grain size distribution of quartz as the protomylonite zone. The frequency of the finer quartz grains (~15 μm), which predominantly constitute the matrix, is higher (~44%) in this zone than in the protomylonite zone (~28%) (Fig. 9b, c, d). Feldspar grains, in the mylonite zone, show a broader grain size distribution, compared to the protomylonite zone. The highest frequency of feldspar grains is at a grain size of 25 μm (Fig. 9c), which is finer than the highest frequency peak in the protomylonites (Fig. 9b). Muscovites also show higher proportion of finer grains (~22 μm) in this zone (Fig. 9d) than in the protomylonites (Fig. 9b). Similarly, biotite grains also have the highest frequency at a finer grain size (~15 μm, Fig. 9d) than in the protomylonites (Fig. 9b).

The high strain mylonite zone is associated with thin bands of ultramylonites that are interfoliated with the mylonites; we will describe the grain size distribution of the ultramylonite bands separately. The high strained mylonites show a further reduction in quartz grain sizes with a maximum frequency at ~11 μm (Fig. 9e). Thus, this zone is marked by the highest frequency of the finest quartz grains with the near absence of the coarser grain size peaks that are seen in the protomylonites and the mylonites (Fig. 9b–d). Feldspar grains in the high strain mylonite zone show an almost unimodal distribution with a maximum frequency at ~21 μm suggesting the absence of feldspar porphyroclasts within this zone (Fig. 9e). Muscovite also shows a unimodal distribution with

Fig. 8. Three dimensional graphs showing the relative proportions of the different microstructures as seen in quartz and feldspars in the (a) protolith, (b) protomylonite zone, (c, d) mylonite zone and (e) High strain mylonite zone. The locations of the fault zone samples are shown in Fig. 5. Note the increase in the proportion of fracturing toward the base of the hanging wall mylonite zone (HWMZ).

a maximum frequency at ~22 μm with the near absence of the coarser grains which are seen in the protomylonites and mylonites (Fig. 9e). Biotite grains show a bimodal distribution with two frequency peaks at ~15 μm and ~34 μm with complete absence of coarser grains that are seen in the protomylonites and mylonites (Fig. 9e).

Finally, the ultramylonite bands present within the high strain mylonite zone are dominantly defined by very fine-grained quartz and a few small plagioclase feldspar grains. Quartz grains present within the ultramylonites show the finest grain size within the hanging wall mylonite zone (HWMZ) with the highest frequency at ~8 μm (Fig. 9f). The few feldspar grains present within this zone show the highest frequency peak at ~15 μm with another peak at ~31 μm (Fig. 9f). Thus, feldspar grains also show the highest distribution of finest grain sizes within the ultramylonites.

The geometric mean grain sizes obtained from these grain size distributions are used to determine the grain-size variation across the mylonite zone (Fig. 10). The geometric mean grain-size vs. distance plot for quartz, feldspar, muscovite and biotite (Fig. 10) shows that the protolith has undergone ~48% grain-size reduction in quartz, ~68% in feldspars, ~22% in muscovite and ~10% in biotite within the HWMZ.

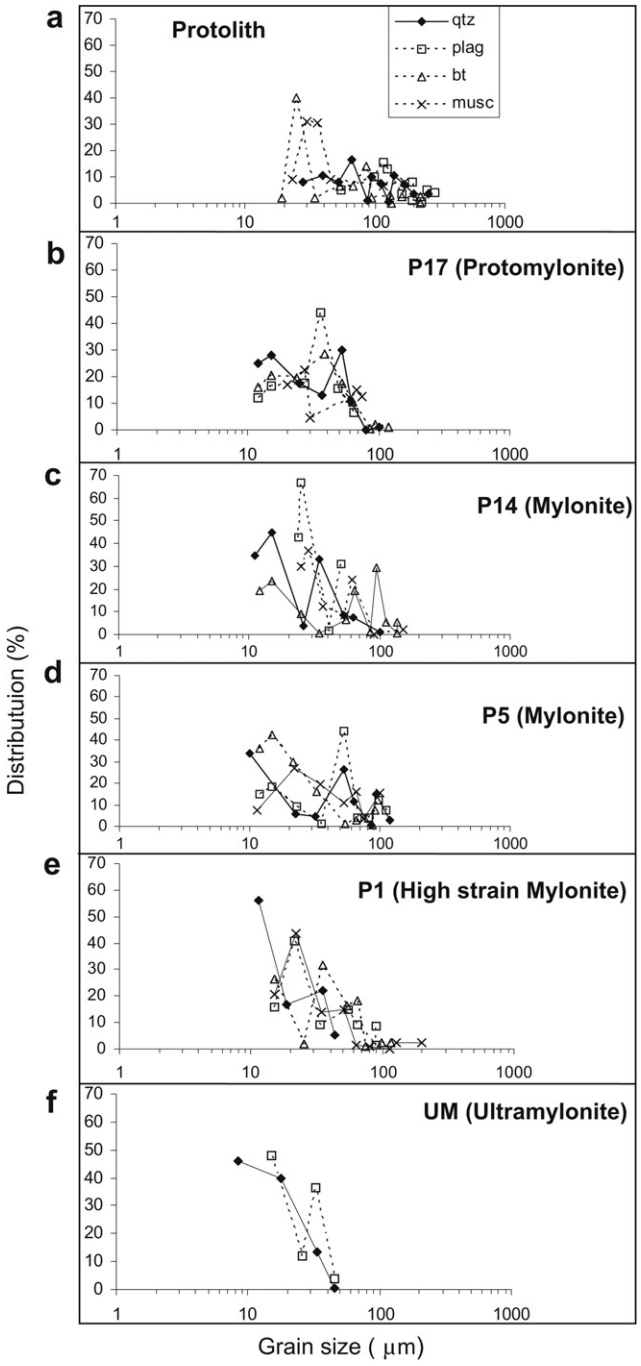

Fig. 9. Logarithmic grain size distribution data for quartz, feldspar, muscovite and biotite of the (a) Lingtse gneiss protolith, (b) protomylonite, (c, d) mylonite, (e) high strain mylonite and (f) ultramylonite. Locations of the fault zone samples are shown in Fig. 5; the ultramylonites are interfoliated with the high strained mylonites.

3.3. Temperature estimate

We have used two independent criteria to broadly estimate the temperature within the HWMZ.

3.3.1. Mineral assemblages

The protolith at Pelling is the Lingtse orthogneiss which does not preserve metamorphic index minerals, making it difficult to estimate temperatures from its mineral assemblage. However, an exposure of a paragneiss ~1 km above the Pelling mylonite zone shows the mineral assemblage,

quartz + feldspar + muscovite + staurolite + garnet + biotite.

The presence of staurolite suggests a temperature of ~530°C–680 °C (Yardley, 1989) for the MCT2 sheet in this part of the Darjeeling – Sikkim Himalaya. The mineral assemblage found within the HWMZ is,

quartz + feldspars + biotite + muscovite + chlorite + epidote

Based on this mineral assemblage, we estimate lower greenschist facies conditions (250°–450 °C) (Yardley, 1989) within the MCT2 mylonite zone at Pelling. In addition, there is evidence of growth of new biotite grains within the mylonite zone suggesting a temperature of ~330 °C within the MCT2 zone. Therefore, we estimate the maximum temperature within the HWMZ to be lower than the highest temperature conditions of greenschist facies, i.e., lower than 450 °C. Sericitization of feldspars clearly provides evidence for presence of fluids within the HWMZ. Thus, higher temperature microstructures observed in quartz likely formed at lower temperature conditions as a result of hydrolytic weakening (Tullis and Yund, 1980).

Close to the footwall contact, i.e., toward the base of the HWMZ, there is evidence of retrogression of biotite to chlorite (Fig. 6f); this suggests temperature conditions to be <330 °C. In addition, the presence of chlorite and epidote suggest that the deformation temperature was at lower greenschist conditions ($T \geq 250$ °C, Mitra,

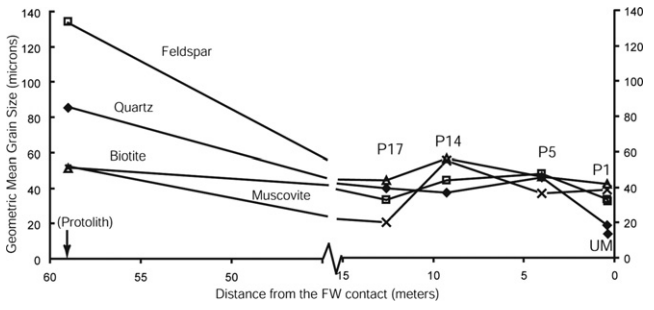

Fig. 10. Plot showing variations in the geometric mean grain sizes of quartz, feldspar, muscovite and biotite with distance from the footwall contact; within the HWMZ, quartz and feldspar have undergone ~48% and 68% grain-size reduction respectively. The sample numbers are shown on the plot; locations of the fault zone samples are shown in Fig. 5.

1993) within the high strain mylonite zone. In other words, there probably was a progressive decrease in temperature toward the base of the HWMZ.

3.3.2. Restored cross-section

Immediately north of our study area, the South Tibetan Detachment system (STDS) lies ~38 km north the MCT1 (Fig. 3); using this and the foliation dip angles within the MCT1 sheet we estimate a first-order thickness of the sheet to be ~24 km (Fig. 3). In addition, the thickness of the MCT2 sheet at Pelling is estimated to be ~5 km. Thus, in the undeformed state, the protolith of the MCT2 zone at Pelling had an overburden of ~29 km (filled star, Fig. 3b). It is important to note, however, that this overburden estimate assumes that the MCT1 sheet was not subjected to erosion between the times of major motions on the MCT1 and MCT2 thrusts, and thus provides a maximum value. Movement on the MCT1 is estimated to initiate at ~22 Ma (Catlos et al., 2004), and that on the MCT2 at ~14 Ma (Catlos et al., 2004); if we assume a uniform rate of erosion since initial emplacement of the MCT1, then the present-day erosion level would suggest that ~9 km of the MCT1 sheet had been eroded (Fig. 3b filled star) and the geothermal gradient had almost completely equilibrated before movement started on the MCT2.

With initiation of movement on the MCT2, the fault climbed up along the footwall ramp bringing hanging wall fault zone rocks (exposed at Pelling) over the footwall (open star, Fig. 3b). For a synorogenic overburden of ~20 km, that includes the thicknesses of both MCT sheets, and a geothermal gradient of ~28° C/km, we arrive at ~560 °C for the deformation temperature. This temperature estimate agrees with the mineral assemblage of the protolith (Section 3.3.1) but is clearly somewhat higher than that suggested by mineral assemblages along the fault zone (<330 °C, Section 3.3.1).

We suggest that the presence of fluids along the fault zone, and further reduction of overburden by erosion during progressive displacement along the MCT2 played a major role in determining the final deformation temperatures in the mylonites.

4. Interpretation

4.1. Microstructures

In this section, we employ the microstructures, described above (Section 3.1), as a tool to understand the various deformation mechanisms that were operating on the fault rocks at Pelling. For example, continuous undulose extinction and deformation twins generally form as a result of conservative motion of dislocations through the crystal lattice and are characteristic of dislocation glide (Rutter, 1983; Schmid, 1982; Tullis and Yund, 1985, 1987). In addition, grain boundaries and presence of impurities may act as stress concentrators and may act as obstacles to dislocation glide giving rise to intragranular fracturing originating at dislocation pile-ups (Mitra, 1978). On the other hand, core-mantle structures, subgrain formation and recrystallization by progressive rotation of subgrains, all suggest nonconservative motion of dislocations and dislocation climb (White, 1976; Rutter, 1983; Schmid, 1982; Tullis and Yund, 1985, 1987). Thus, based on frequencies of various microstructures (Fig. 8), we can plot the likely proportions of grains of quartz and feldspars showing different grain-scale deformation mechanisms within the hanging wall mylonite zone (HWMZ) (Fig. 11a,b).

Based on their finer grain sizes (<30 μm), equant shapes and slightly wavy to straight grain boundaries forming triple junctions (Fig. 6b), we interpret the matrix forming quartz grains as recrystallized quartz grains. These recrystallized quartz grains are generally of the same size as the subgrains suggesting that they formed by progressive rotation of the subgrains (White, 1976). There is a progressive decrease in the proportion of quartz grains showing subgrain formation toward the base of the mylonite zone, which we interpret to be the result of increasing proportion of recrystallized quartz grains toward the base. The recrystallized quartz grains throughout the mylonite zone continue to show undulose extinction suggesting that quartz grains have continuously accommodated deformation by dislocation glide and recovery by dislocation climb through a process of dynamic recrystallization (Fig. 11a).

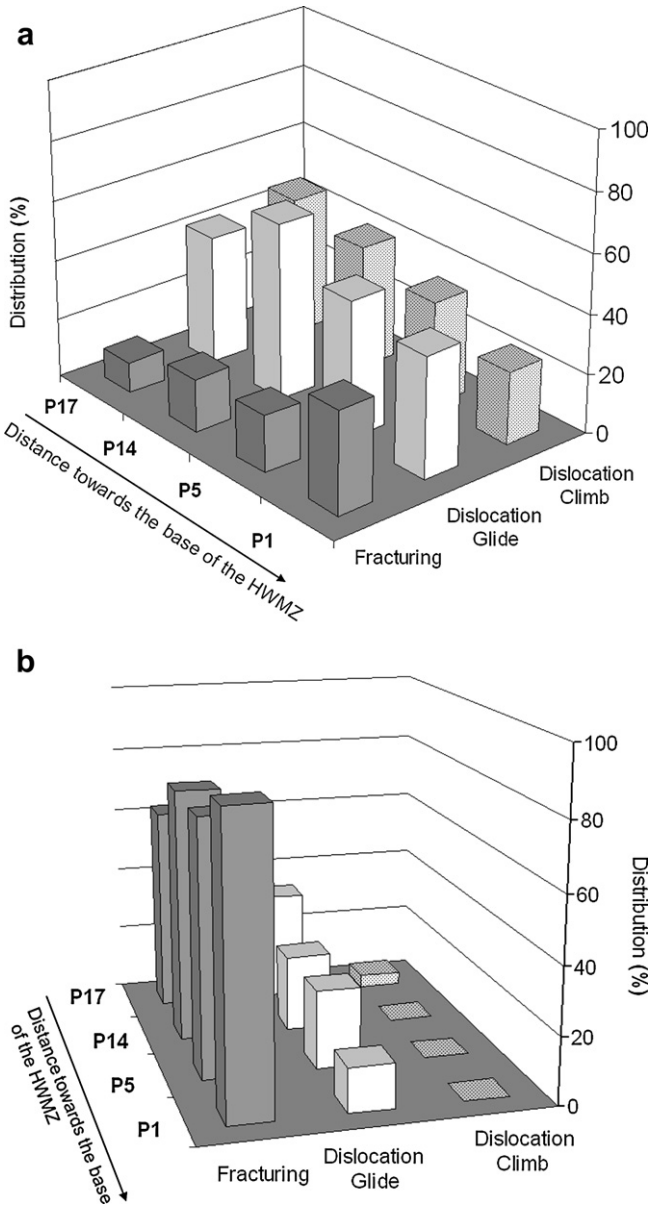

Fig. 11. (a) Three dimensional plot showing the relative proportions of quartz grains showing different deformation mechanisms within the hanging wall mylonite zone (HWMZ) at Pelling. Quartz shows approximately uniform proportion of dislocation glide throughout the HWMZ; proportion of dislocation climb decreases toward the base of the HWMZ and fracturing increases toward the base. Sample numbers are shown in the plot and their locations are shown in Fig. 5. (b) Three dimensional plot showing the relative proportions of feldspar grains showing different deformation mechanisms within the hanging wall mylonite zone (HWMZ) at Pelling. The plot shows that fracturing is the most dominant deformation mechanism that progressively increases toward the base of the HWMZ and dislocation glide progressively decreases toward the base of the HWMZ. Sample locations are shown in Fig. 5.

The geometric mean grain size plot of quartz (Fig. 10) shows ~48% grain-size reduction from the protolith to the HWMZ. The prevalence of quartz recrystallization suggests that most of this grain-size reduction takes place by dislocation creep in quartz. In addition, Fig. 11 shows an increase in fracturing in quartz from ~10% of quartz grains in the protomylonite zone to ~30% of quartz grains at the base of the HWMZ. The fractures cross cut the mylonitic foliation, overprint the plastic deformation features, and cause some grain-size reduction. We interpret most of this fracturing to be related to late stage cataclasis along the fault zone resulting from a change in deformation conditions as the fault rocks were progressively unroofed by erosion.

Feldspar grains, on the other hand, deform dominantly by fracturing (Fig. 11b) within the mylonite zone. Most of this fracturing overprints the earlier plastic deformation features in the feldspar grains that are seen in the protolith. There is an increase in the number of feldspar grains showing patchy extinction that is closely associated with intragranular fracturing, toward the base of the HWMZ. We interpret these fractures to be most likely related to dislocation pile-ups at obstructions such as grain boundaries (e.g. Mitra, 1978). The proportion of feldspar grains showing fracturing increases from ~64% in the protomylonite zone to ~88% at the base of mylonite zone.

Sericitization of feldspars is seen throughout the mylonite zone and is strongest toward the base of the zone; the requirement of H_2O for this feldspar breakdown reaction suggests an increase in the degree of fluid movement toward the base of the HWMZ. We interpret that the increasing fracturing toward the base of the HWMZ enhanced the permeability and increased the surface area of the feldspar grains making them more susceptible to chemical reactions (Mitra, 1978; Etheridge et al., 1983). Thus, the feldspar grains were deformed by both mechanical and chemical processes. The latter led to the formation of micas that have weaker bonding between (001) planes than strongly bonded framework silicates; this would result in higher porosity in the rock (Etheridge et al., 1983). Hence, an increased porosity probably led to an effective interconnected porosity that increased permeability and enhanced fluid mobility (Etheridge et al., 1983, 1984; Newman and Mitra, 1993) within the HWMZ. Thus, fracturing and fluid flow together enhanced the retrogressive reactions in feldspars within the HWMZ (Mitra, 1978, 1992; White and Knipe, 1978; White et al., 1980; Gilotti, 1992).

In summary, quartz has undergone grain-size reduction within the HWMZ mainly by dislocation glide and climb while microfracturing is the dominant grain-size reduction mechanism in feldspars.

4.2. Quartz deformation mechanism map

The deformation behavior during initial movement along a greenschist grade fault zone is typically controlled by the stronger phases, such as quartz and feldspar, when they are present in sufficient volumes to form a stress-supporting framework. Progressive evolution of the fault zone is generally associated with decreasing grain sizes during mylonitization of the fault rocks. Sufficient grain-size reduction may lead to strain softening of the minerals due to grain-size sensitive creep processes and consequent weakening of the fault zone; at this stage the weakest phases may control the overall deformation of the fault zone. In the Pelling HWMZ, along with quartz and feldspar grains, that typically form the strong phase of fault rocks, there is a significant proportion of weaker phase defined by micas that resulted from the syntectonic reaction breakdown of feldspar grains. In this section, we examine the relative roles of quartz and feldspar (the stronger phase) and micaceous minerals (the weaker phase) in controlling the strength of the fault rocks at Pelling.

Although there are both plagioclase and alkali feldspars present in the protolith of the MCT2 zone, there is a progressive reduction in the proportion of feldspars from ~26% in the protolith to ~13% within the HWMZ. Feldspar grains have low contiguity, and do not act as a stress-supporting framework (Mitra, 1978, 1992). In other words, feldspars play a very limited role in the overall rheologic behavior of the mylonite zone. Therefore, we have used quartz as the representative initially stronger phase of this polyphase system to examine its role in the deformation history of the MCT2 mylonite zone.

Quartz has the highest modal percentage in both the undeformed protolith (~40%) and in the HWMZ (~38%) and thus forms the main constituent of the strong phase. Additionally, its mechanical properties are well studied (e.g., White, 1976; Rutter, 1976; Farver and Yund, 1991) making it possible to study its deformation behavior during fault zone evolution. We have constructed a grain size vs. stress deformation mechanism map (Schmid, 1982) for quartz, at a constant temperature to allow us to study the effect of its grain-size reduction on the mechanical behavior of the mylonites.

Based on our estimate of temperature (Section 3.3), the deformation mechanism map for quartz is constructed for a temperature of 300 °C in the presence of fluids (Fig. 12) using well-known flow law parameters (Rutter, 1976; Farver and Yund, 1991; Passchier and Trouw, 2005). Since our temperature estimates suggest that there was a progressive decrease in temperature from the hanging wall protolith toward the base of the mylonite zone, we restrict our analysis to the fault zone rocks and thus do not consider the coarser quartz grains of the protolith that deformed at higher temperatures. We estimated a grain size of 64.66 μm and stress of 1.77×10^{-4} MPa for the triple point where all three deformation mechanisms of dislocation creep, grain boundary diffusion and lattice diffusion operate simultaneously in quartz in the presence of fluids.

Assuming a total displacement of 122 km for the MCT2 thrust sheet over a period of ~3 Ma (Bhattacharyya, 2010), a thickness of ~373 m for the HWMZ, and deformation by simple shear within

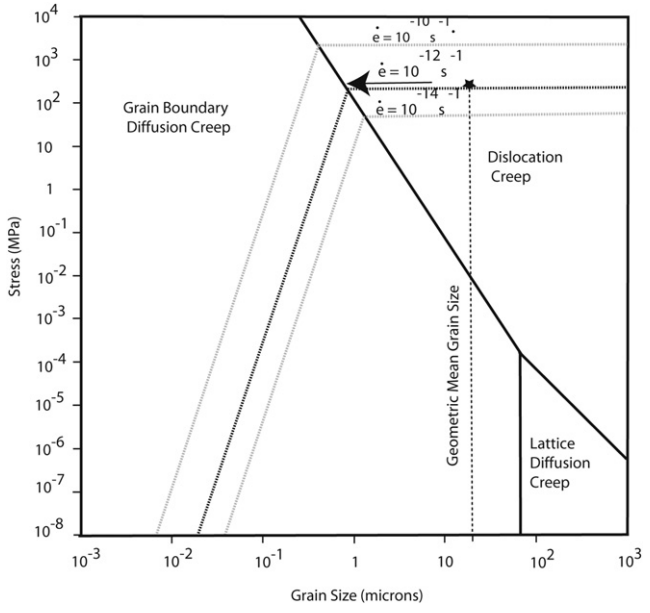

Fig. 12. Deformation mechanism map of Quartz at 300 °C, in the presence of fluid (Schmid, 1982). The geometric mean grain size of quartz from the fault rocks plot within the dislocation creep field at an average strain rate of 10^{-12} s^{-1}.

the zone, we arrive at an average strain rate on the order of 10^{-12} s^{-1} for the MCT2 zone. For this strain rate, the geometric mean grain size of the quartz grains from all the fault rocks plot within the dislocation creep field on the deformation mechanism map. This suggests that recrystallization was the dominant deformation mechanism for quartz within the MCT2 zone. In addition, the recrystallized quartz grains were continuously deformed by dislocation creep (i.e., glide and climb) as is seen from microstructures (described earlier in Section 1). However, even though there was progressive grain-size reduction by recrystallization during the deformation, the deformation mechanism map clearly shows that the recrystallized grain size was not sufficiently small for the dominant deformation mechanism in quartz to switch to grain size-sensitive, diffusion controlled creep mechanisms (DeBresser et al., 2001). Therefore, the recrystallized quartz matrix within the HWMZ at Pelling was not significantly weakened during the deformation, and quartz did not dominantly control the strength of the fault rocks in the MCT2 zone at Pelling. In the following section, we focus our attention on the micas to examine their role in controlling the deformation.

4.3. Role of micas

At Pelling, there is a significant change in mineralogical composition from the protolith to the HWMZ. In addition to a reduction in feldspar content (Section 4.2) (Fig. 7), the modal percentage of muscovites increased from ~6% in the protolith to ~22% within the HWMZ, and quartz increased from 39% to 42%. This inverse relationship between the decreasing proportion of feldspars and increasing proportion of Quartz and Mica shows that retrogression of feldspars to Quartz and Micas, in the presence of fluids, was a prominent process within the HWMZ.

In the protolith, the modal percentage of the intrinsically weak matrix, made up of muscovite, biotite and chlorite, is ~35% (Fig. 13). Within the HWMZ, the modal percentage of weak matrix increases toward the base, from ~37% in the protomylonite zone to ~63% in the high strain mylonite zone (Fig. 13). The proportion of weak matrix in the highly deformed mylonite is greater than the rheologically critical matrix percentage (Tharp, 1983; Gilotti, 1992), so that ultimately the deformation was controlled by the matrix fraction within the mylonite zone. We propose that, along with the factors that are described in Section 4.1, the lithology of the footwall rocks played a critical role in generating the large amounts of intrinsically weak matrix within the fault zone at Pelling. The greenschist grade metasedimentary footwall rocks of slates, phyllites, along with quartzites, had the necessary porewater fluids that were released during the deformation of the MCT2. In addition, there was an increase in proportion of fracturing within the feldspar grains with ~88% of all feldspar grains showing fracturing toward the base of the mylonite zone (Fig. 11b). The increase in fracturing decreased the grain sizes of feldspar grains and, in turn, increased the surface area of the feldspar grains. Thus, an increase in fluid/rock contact area (Newman and Mitra, 1994) enhanced the process of sericitization; this resulted in the production of large volume of matrix within the HWMZ. In addition, porphyroclasts, when present, tend to act as obstacles to accommodation of shear strain by the intrinsically weak matrix. Thus, the porphyroclasts act as stress concentrators (Mitra, 1992) and, in turn, continue to result in generation of further fracturing. Therefore, the almost complete absence of porphyroclasts near the base of the HWMZ, and a large volume of intrinsically weak matrix suggest that grain-size reduction and sericitization of feldspar grains continued even when the weak matrix dominantly took up the shear strain (Mitra, 1992) at Pelling. Thus, at Pelling, the strength of fault rocks decreased as the proportion of intrinsically weak matrix progressively increased within the HWMZ, eventually exceeding the rheologically critical matrix percentage. This localized the deformation along thin weak zones of intense deformation allowing very large displacements to take place along a relatively thin fault zone. Thus, the MCT2 mylonite zone represents a Type II fault zone (Means, 1984; Mitra, 1992).

5. Discussion

In low-grade mylonite zones, there is an empirical linear relationship on a log–log plot between the thickness (T) of a mylonite zone and the displacement (D) along it (Hull, 1988) (Fig. 14). As mentioned in Section 3, the maximum thickness of the MCT2 zone at Pelling is ~373 m based on the nearest locations of hanging wall and footwall protoliths, while the exposed HWMZ gives a minimum thickness of ~19 m. Plotting this range of thicknesses on the thickness–displacement plot (Fig. 14) suggests that the MCT2 zone should have a maximum displacement of ~25 km, if it followed the patterns suggested by other low-grade mylonite zones. However, based on the balanced cross section (Fig. 3, Mitra et al., 2010), the MCT2 has a total displacement of ~122 km (Bhattacharyya, 2010) in the Darjeeling – Sikkim Himalaya, and plots outside the compiled dataset for low-grade mylonite zones on the T-D plot (Fig. 14). This corroborates our microstructural observation that the MCT2 zone has undergone strain softening and represents a Type II fault zone (Means, 1984; Mitra, 1992) in which the large displacement has been localized along a relatively thin zone.

Myonitization of many polyphase rocks results in the production of weak matrix that plays a key role in controlling the deformation mechanisms within mylonite zones (Mitra, 1978; Kerrich et al., 1980; Gilotti, 1992). For a polyphase mylonite, Gilotti (1992) recognized two different classes of weak matrix that might develop: (i) an intrinsically weak matrix made up of minerals of low strength, and (ii) a fine-grained aggregate deforming by grain size-sensitive creep mechanisms (Schmid, 1982; Mitra, 1984). The role of the latter in controlling deformation was demonstrated in the

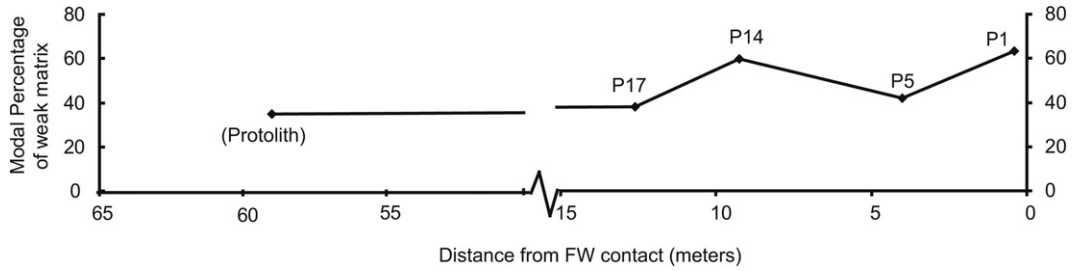

Fig. 13. Plot showing variation of modal percentages of the intrinsically weak matrix defined by muscovite, biotite and chlorite with distance from the footwall contact. Fault zone sample numbers are shown on the plot and their locations are shown in Fig. 5.

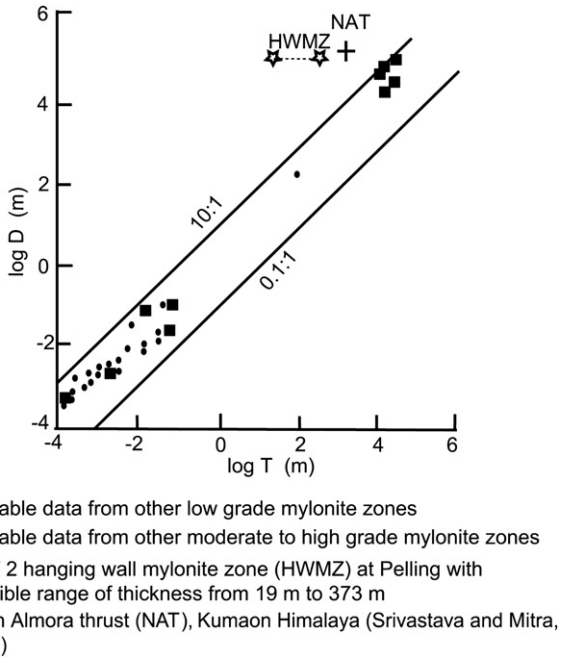

Fig. 14. Log–log thickness (T) – displacement (D) plot for mylonite zones (after Hull, 1988) showing a logarithmic linear relationship between the two. Available data from other mylonite zones are shown. The MCT2 zone plots outside the available dataset of low-grade mylonite zones suggesting that the MCT2 zone has undergone strain softening along it.

Swedish Caledonides for the quartzo-feldspathic mylonites along the Särv thrust (Gilotti and Kumpulainen, 1986) that accommodated ~100 km displacement along a 10–100 m thick mylonite zone once the mylonites reached a rheologically critical matrix fraction (RCMF) (Gilotti, 1992). The concept of an RCMF for an intrinsically weak matrix bears some discussion: significant weakening of a rock may occur only if the weak phase is an order of magnitude weaker than the strong phase (Tharp, 1983; Jordan, 1987). While this condition might be satisfied in rocks with a salt or anhydrite matrix, it is not as easily obtained in quartzo-feldspathic mylonites.

Single crystals of biotite are approximately twice as strong as muscovite (Kronenberg et al., 1990; Mares and Kronenberg, 1993). This suggests that mylonites developing muscovite by feldspar breakdown from quartz-feldspar-biotite gneiss will be somewhat weaker than the protolith. Both biotite and muscovite are weakest when their cleavage is oriented ~45° to the maximum compressive stress, that is parallel to the maximum shearing stress. In foliated rocks, the foliation is often defined by the parallel arrangement of micaceous minerals. Deformation experiments on foliated quartz-feldspar-mica gneisses and schists (Shea and Kronenberg, 1993) have shown that these rocks are weakest when the foliation is at ~45° to the maximum compression, i.e. parallel to maximum shearing stress. In these rocks, deformed at low temperatures, the deformation appears to change to ductile, low strength behavior when the mica content exceeds 30–40% by volume and the strength decreases to as much as 4 times lower in rocks with >50% mica as compared to rocks with ~10% mica (Shea and Kronenberg, 1993). On the other hand, in quartz-mica compacts deformed at temperatures high enough for quartz to recrystallize by dislocation climb (Regime 2 of Hirth and Tullis, 1992) quartz is less than 2 times as strong as mica and there is little effect on overall rock strength even at 50% mica content (Tullis and Wenk, 1994).

The MCT2 zone at Pelling shows evidence of a fine-grained matrix composed of recrystallized quartz grains and micas. Our analysis shows that the quartz grains deformed by subgrain rotation (Regime 2 of Hirth and Tullis, 1992), and grain-size remained within the dislocation creep field (Fig. 12); thus, the recrystallized quartz grains did not reach fine enough grain size to have deformed by grain size-sensitive diffusion mechanisms (e.g. DeBresser et al., 2001). But, the MCT2 zone at Pelling also shows a progressive increase in the proportion of the micaceous matrix, defined by muscovite, chlorite and biotite, from the protolith/protomylonite (~35–38%), to the high strain mylonites (~63%) (Fig. 13). It should be noted, however, that under the deformation conditions suggested by the microstructures observed in quartz, the micaceous minerals may not have been significantly weaker than quartz and their presence may not have significantly weakened the rock (Tharp, 1983). Handy (1990) suggests that in rocks with low relative strengths of the strong and weak phases, type 2 deformation leads to the formation of elongated boudins of the strong phase in a weak matrix. In a quartz-mica mylonite this would impart a strong foliation defined by elongated quartz lenses and parallelism of mica grains in the matrix. Such a strong foliation would lead to geometric weakening (foliation weakening, Jordan, 1987), particularly in shear zones where the maximum shearing stress would be approximately parallel to the foliation and the mica cleavage planes. We suggest that the weakening (strain softening) of the mylonite zone as a whole could be a result of a combination of the RCMP and geometric weakening due to the parallelism of mica grains. This, in turn, would have led to localized deformation along a relatively thin zone.

It is interesting to note here that the North Almora thrust (NAT) zone (Valdiya, 1980; Srivastava and Mitra, 1996), in the Kumaon–Garhwal Himalaya, is structurally equivalent to the MCT2 zone of the Darjeeling – Sikkim Himalaya. The NAT records a minimum translation of ~150 km (Srivastava and Mitra, 1994), and the hanging wall mylonite zone near the town of Takula is ~2.2 km thick. It evolved at a higher metamorphic grade (400°C-600 °C) (Srivastava and Mitra, 1996) than the Pelling MCT2 zone (250 °C–350 °C). The NAT zone has an inverted thermal profile that was explained as due to syntectonic cooling of the hanging wall during thrusting (Srivastava and Mitra, 1996). Both quartz and feldspar grains show high temperature plastic deformation structures (i.e., recrystallization) in the protomylonites and indicate highest temperatures (~600 °C) away from the base of the NAT mylonite zone; the temperatures are estimated to decrease through the mylonite (~500 °C) to the ultramylonites (~400 °C) at the base (Srivastava and Mitra, 1996). Feldspars show extensive evidence of breakdown to quartz and muscovite in the presence of fluids, thereby causing reaction softening in both the mylonites and ultramylonites, and strong foliation development. Thus, the strain softening mechanisms in Kumaon and Sikkim are very similar in spite of significantly different pressure-temperature conditions obtained from both microstructural evidence and restored balanced cross-sections in the two areas, and minor differences in lithology and grain-size of the protoliths (Srivastava, 1993). Thus, apart from the variations in the protoliths at these two locations, the higher temperature of the NAT mylonite zone explains the high temperature plastic deformation structures in feldspar grains in the protomylonite at Takula, while similar structures were not recorded in the Pelling mylonite zone. But, ultimately, feldspar breakdown to quartz and muscovite led to strain softening in both areas at somewhat different temperatures.

These two locations along the MCT are separated by a distance of ~1000 km along a 2500 km long fault zone, and similarities and differences in deformation mechanisms are difficult to address over

such long distances. However, the similarities in softening mechanisms at these two locations, in spite of differences in pressure-temperature conditions and lithologies involved, suggest that we should expect similar processes in other locations along this major fault zone.

Defining the location of the MCT has been the focus of many studies in the Himalayan FTB. In Sikkim, two distinct thrust faults are well exposed within the Greater Himalaya. We have defined the MCT2 as the structurally lower thrust that places the amphibolite grade Lingtse gneiss of the GHS over the greenschist grade Daling Formation of the LHS. In our interpretation, the MCT2 is a footwall imbricate of the structurally higher MCT1, and developed later than the MCT1 in a normal, break-forward sequence (Mitra et al., 2010; Bhattacharyya, 2010). It is important to note that in eastern Nepal, the MCTII or the Khumbh thrust (Bordet, 1961; Hashimoto et al., 1973; Lombardo et al., 1993; Pognante and Benna, 1993; Goscombe et al., 2006) is defined as the structurally higher thrust, lying at the base of the "Tibetan slab" and is equivalent to the MCT1 thrust, as we have defined it in Sikkim (Mitra et al., 2010). In addition, there is evidence of lateral variation in P-T conditions on the MCT2 fault along the length of the Himalayan arc, as we have already discussed.

6. Conclusions

In the Darjeeling – Sikkim Himalaya, two distinct thrusts are exposed in the GHS, the structurally higher MCT1 and the structurally lower MCT2, together forming the MCT. At Pelling, the MCT2 zone is exposed at the contact between the Lingtse gneiss in the hanging wall and the Daling slates in the footwall and is ~373 m thick and exposes ~19 m of strongly deformed hanging wall mylonites. Within the mylonite zone, quartz has undergone ~48% grain-size reduction by dislocation creep and feldspars have undergone ~68% grain-size reduction dominantly by fracturing. In addition, the amphibolite grade MCT sheet has undergone fluid-assisted retrogression within the MCT2 mylonite zone. Within the mylonite zone, there is evidence of reaction softening of feldspars to Quartz and Micas by sericitization that produced large proportions of intrinsically weak matrix; the matrix proportion within the mylonite zone increased toward the base and became greater than the rheologically critical matrix percentage. However, under the deformation conditions indicated by quartz microstructures, the strength difference between quartz (strong phase) and mica (weak phase) is not sufficiently large to have caused significant weakening of the fault zone as a whole. Development of a strong foliation defined by parallel mica grains would have resulted in geometric weakening (foliation weakening). This, in combination with RCMF, resulted in weakening of the mylonite zone, i.e., strain softening, that localized the deformation along a relatively thin zone. Therefore, the MCT2 mylonite zone at Pelling is an example of an internal fault zone where the increase in proportion of intrinsically weaker phases led to fault zone weakening that allowed a large translation of more than 100 km of the MCT2 sheet.

Acknowledgments

This work was supported by NSF grant EAR-0439999 to G. Mitra and grants from the Geological Society of America and the Nuria Pequera Fellowship of the University of Rochester to K. Bhattacharyya. We thank the reviewers, J. Newman and S. Wojtal, and the editor, J. Hippertt, for their detailed and thoughtful comments that significantly improved the quality of the paper. We thank Gerry Kloc for preparing excellent thin sections for this study.

References

Acharyya, S.K., 1971. In: Recent Geological Studies in the Himalaya. Structure and stratigraphy of the Darjeeling Frontal zone, eastern Himalaya, vol. 24. Geological Survey of India Miscellaneous Publication (1), pp. 71–90.
Acharyya, S.K., Ray, K.K., 1977. Geology of the Darjeeling–Sikkim Himalaya. In: Guide to Excursion No. 3, Fourth International Gondwana Symposium. Geological Survey of India, Calcutta, pp. 1–25.
Bhattacharyya, K., Mitra, G., 2009a. A new kinematic evolutionary model for the growth of a duplex – an example from the Rangit duplex, Sikkim Himalaya, India. Gondwana Research 16, 697–715.
Bhattacharyya, K., Mitra, G., 2009b. The MCT Zone from the Sikkim Himalaya: An Example of a Retrogressed Mylonite Zone. In: Geological Society of America Abstracts with Programs, vol. 41, pp. 691.
Bhattacharyya, K., 2010. Geometry and Kinematics of the Fold-Thrust Belt and Structural Evolution of the Major Himalayan Fault zones in theDarjeeling – Sikkim Himalaya, India. PhD thesis, University of Rochester, pp. 1–263.
Bordet, P., 1961. Recherches Geologiques Dans l'Himalaya du Nepal, Region du Makalu. Editions du Centre National Recherches Scientifiques, Paris, pp. 275.
Bordet, P., Colchen, M., LeFort, P., 1972. Some features of the geology of the Annapurna Range, Nepal Himalaya. Himalayan Geology 2, 537–563.
Boyer, S.E., Elliott, D., 1982. Thrust systems. American Association of Petroleum Geologists Bulletin 66, 1196–1230.
Boyer, S.E., Geiser, P.A., 1987. Sequential Development of Thrust Belts; Implications for Mechanics and Cross Section Balancing. In: Geological Society of America Abstracts with Programs, vol. 19 597.
Butler, R.W.H., Coward, M.P., 1984. Geological constraints, structural evolution, and deep geology of the Northwest Scottish Caledonides. Tectonics 3, 347–365.
Catlos, E.J., Harrison, T.M., Kohn, M.J., Grove, M., Ryerson, F.J., Manning, C.E., Upreti, B.N., 2001. Geochronologic and thermobarometric constraints on the evolution of the main central thrust, central Nepal Himalaya. Journal of Geophysical Research 106, 16,177–16,204.
Catlos, E.J., Dubey, C.S., Harrison, T.M., Edwards, M.A., 2004. Late Miocene movement within the Himalayan main central thrust shear zone, Sikkim, north-east India. Journal of Metamorphic Geology 22, 207–226.
Daniel, C.G., Hollister, L.S., Parrish, R.R., Grujic, D., 2003. Exhumation of the main central thrust from lower crustal depths, Eastern Bhutan Himalaya. Journal of Metamorphic Geology 21, 317–334.
DeBresser, J.H.P., Ter Heege, J.H., Spiers, C.J., 2001. Grain size reduction by dynamic recrystallization: can it result in major rheological weakening? International Journal of Earth Sciences 90, 28–45.
DeCelles, P.G., Gehrels, G.E., Quade, J., Ojha, T.P., Kapp, P.A., Upreti, B.N., 1998. Neogene Foreland Basin Deposits, Erosional Unroofing, and the Kinematic History of the Himalayan Fold-thrust Belt, Western Nepal. In: Geological Society America Bulletin, vol. 110 2–21.
DeCelles, P.G., Robinson, D.M., Quade, J., Ojha, T.P., Garzione, C.N., Copeland, P., Upreti, B.N., 2001. Stratigraphy, structure and tectonic evolution of the Himalayan fold-thrust belt in western Nepal. Tectonics 20, 487–509.
Elliott, D., Johnson, M.R.W., 1980. Structural evolution in the northern part of the Moine thrust belt. Transactions of the Royal Society of Edinburgh. Earth Sciences 71, 69–96.
Etheridge, M.A., Wall, V.J., Vernon, R.H., 1983. The role of the fluid phase during regional metamorphism and deformation. Journal of Metamorphic Geology 1, 205–226.
Etheridge, M.A., Wall, V.J., Cox, S.F., Vernon, R.H., 1984. High fluid pressures during regional metamorphism and deformation: implications for mass transport and deformation mechanisms. Journal of Geophysical Research 89, 4344–4358.
Evans, J.P., 1991. Textures, deformation mechanisms and the role of fluid in the cataclastic deformation of granitic rocks. In: Knipe, R.J., Rutter, E.H. (Eds.), Geological Society of London Special Publications, 54, pp. 29–41.
Evans, J.P., 1993. Deformation mechanisms and kinematics of a crystalline-cored thrust sheet: the Washakie thrust system, Wyoming. In: Schmidt, C.J., Chase et al., Chase, R., Erslev, E.A. (Eds.), Geological Society of America Special Paper, 280, pp. 147–161.
Farver, J.R., Yund, R.A., 1991. Oxygen diffusion in quartz; dependence on temperature and water fugacity. Chemical Geology 90, 55–70.
Gangopadhyay, P.K., Ray, S., 1980. Tectonic framework of the Rangit window around Namchi, South Sikkim. Himalayan Geology 10, 338–353.
Gansser, A., 1964. Geology of the Himalayas. Interscience, Wiley, New York. 1–289.
Gansser, A., 1983. Geology of the Bhutan Himalaya. Birkhauser Verlag, Basel, p. 181.
Gilotti, J.A., Kumpulainen, R., 1986. Strain softening induced ductile flow in the Särv thrust sheet, Scandinavian Caledonides. Journal of Structural Geology 8, 441–455.
Gilotti, J.A., 1992. The Rheologically Critical Matrix in Arkosic Mylonites Along the Särv Thrust, Swedish Caledonides. In: Mitra, S., Fisher, G. (Eds.), Structural Geology of Fold and Thrust Belts. Johns Hopkins University Press, Baltimore, pp. 145–160.
Goscombe, B., Gray, D., Hand, M., 2006. Crustal architecture of the Himalayan metamorphic front in eastern Nepal. Gondwana Research 10, 232–255.
Hashimoto, S., Ohta, Y., Akiba, C., 1973. Geology of the Nepal Himalayas. Saikon, Tokyo.
Handy, M.R., 1990. The solid-state flow of polymineralic rocks. Journal of Geophysical Research 95, 8647–8661.
Heim, A., Gansser, A., 1939. Central Himalaya, geological observations of the Swiss expedition. Memoir of Society Helveticae Science Nat vol. 73 (1), 1–245.

Hirth, G., Tullis, J., 1992. Dislocation creep regimes in quartz aggregates. Journal of Structural Geology 14, 145–159.
Hull, J., 1988. Thickness–displacement relationships for deformation zones. Journal of Structural Geology 10, 431–435.
Huyghe, P., Galy, A., Mugnier, J.L., Lanord, C., 2001. Propagation of the thrust system and erosion in the Lesser Himalaya: geochemical and sedimentological evidence. Geology 29, 1007–1010.
Imamura, L., Bhattacharyya, K., Mitra, G., 2011. Microstructural Evidence for Strain-softening along the Main Central Thrust Zone in the Darjeeling-Sikkim Himalaya. In: Geological Society of America Abstracts with Programs, vol. 43-1, pp. 148.
Jordan, P.G., 1987. The deformation behaviour of bimineralic limestone-halite aggregrates. Tectonophysics 135, 185–197.
Kerrich, R., Allison, I., Barnett, R.L., Moss, S., Starkey, J., 1980. Microstructural and chemical transfprmations accompanying deformation of granite in a shear zone at Mieville, Switzerland: with implications for stress corrosion cracking and superplastic flow. Contributions to Mineralogy and Petrology 73, 221–242.
Kronenberg, A.K., Kirby, S.H., Pinkston, J.C., 1990. Basal slip and mechanical anisotropy of biotite. Journal of Geophysical Research 95, 19257–19278.
Le Fort, P., 1975. Himalaya: the collided range: present knowledge of the continental arc. American Journal of Science 275A, 1–44.
Le Pichon, X., Fournier, M., Jolivet, L., 1992. Kinematics, topography, shortening and extrusion in the India–Eurasia collision. Tectonics 11, 1085–1098.
Lombardo, B., Pertusati, P.C., Borghi, S., 1993. Geology and tectonomagmatic evolution of the eastern Himalaya along Chomolungma-Makalu transect. In: Treloar, P.J., Searle, M.P. (Eds.), Himalayan Tectonics. Geological Society of London Special Publication, vol. 74, pp. 341–355.
Mallet, F., 1875. On the geology and mineral resources of the Darjeeling district and the western Duars. Memoirs of the Geological Survey of India 11, 1–50.
Mares, V.M., Kronenberg, A.K., 1993. Experimental deformation of muscovite. Journal of Structural Geology 15, 1061–1075.
Martin, A.J., DeCelles, P.G., Gehrels, G.E., Patchett, P.J., Isachsen, C., 2005. Isotopic and Structural Constraints on the Location of the Main Central Thrust in the Annapurna Range, Central Nepal Himalaya. In: Geological Society of America Bulletin, vol. 17 926–944.
McQuarrie, N., DeCelles, P.G., 2001. Geometry and structural evolution of the central Andean Backthrust Belt, Bolivia. Tectonics 17, 203–220.
McQuarrie, N., Robinson, D., Long, S., Tobgay, T., Grujic, D., Gehrels, G., Ducea, M., 2008. Preliminary Stratigraphy and Structural architecture of Bhutan: implications for the along strike architecture of the Himalayan system. Earth and Planetary Science Letters 272, 105–117.
Means, W.D., 1984. Shear Zones of Types I and II and Their Significance for Reconstruction of Rock History. In: Geological Society of America Abstracts, vol. 16, p. 50.
Medlicott, H.B., 1864. On the geological structure and relations of the southern portion of the Himalayan ranges between the Rivers Ganges and the Ravee. Memoir Geological Survey of India 3, 102.
Mitra, G., 1978. Ductile deformation zones and mylonites: the mechanical processes involved in the deformation of crystalline basement rocks. American Journal of Science 278, 1057–1084.
Mitra, G., 1984. Brittle to ductile transition due to large strains along the White Rock thrust, Wind River Mountains, Wyoming. Journal of Structural Geology 6, 51–61.
Mitra, G., 1992. Deformation of granitic basement rocks along fault zones at shallow to intermediate crustal levels. In: Mitra, S., Fisher, G.W. (Eds.), Structural Geology of Fold and Thrust Belts, pp. 123–144.
Mitra, G., 1993. Deformation processes in brittle deformation zones in granitic basement rocks: a case study from the Torrey Creek area, Wind River Mountains. In: Schmidt, C., Chase, R., Erslev, E. (Eds.), Basement Behavior in Rocky Mountain Foreland Structure. Geological Society of America Special Paper, 280, pp. 177–195.
Mitra, G., Ismat, Z., 2001. Microfracturing associated with reactivated fault zones and shear zones: what can it tell us about deformation history? In: Holdsworth, R.E., Strachan, R.A., Magloughlin, J.F., Knipe, R.J. (Eds.), The Nature and Tectonic Significance of Fault Zone Weakening Geological Society of London Special Publication, vol. 186, pp. 113–140.
Mitra, G., Bhattacharyya, K., Mukul, M., 2010. The Lesser Himalayan duplex in Sikkim: implications for variations in Himalayan shortening. Special Issue of Journal of Geological Society of India 75, 289–301.
Mukul, M., 2000. The geometry and kinematics of the Main Boundary Thrust and related neotectonics in the Darjiling Himalayan fold-and-thrust belt, West Bengal, India. Journal of Structural Geology 22, 1261–1283.
Newman, J., Mitra, G., 1993. Lateral variations in fault zone thickness as influenced by fluid-rock interactions, Linville Falls fault, North Carolina. Journal of Structural Geology 15, 849–863.
Newman, J., Mitra, G., 1994. Fluid-influenced Deformation and Recrystallization of Dolomite at Low Temperatures along a Natural Fault Zone, Mountain City Window, Tennessee. In: Geological Society of America Bulletin, vol. 106 1267–1280.
Oldham, T.A., 1883. Catalogue of Indian earthquakes. Memoir of Geological Survey of India 19, 163–215.
Parrish, R., Hodges, K.V., 1996. Isotopic Constraints on the Age and Provenance of the Lesser and Greater Himalayan Sequences, Nepalese Himalaya. In: Geological Society of America Bulletin, vol. 108 904–911.
Passchier, C.W., Trouw, R.A.J., 2005. Microtectonics. Springer-Verlag, Berlin, p. 366.
Pearson, O.N., DeCelles, P.G., 2005. Structural geology and regional tectonic significance of the Ramgarh thrust, Himalayan fold-thrust belt of Nepal. Tectonics 24, TC4008.
Pêcher, A., 1975. The main central thrust of the Nepal Himalaya and the related metamorphism in the Modi-Khola cross-section (Annapurna Range). Himalayan Geology 5, 115–131.
Pognante, U., Benna, P., 1993. Metamorphic Zonation, Migmatization, and Leucogranites along the Everest Transect (Eastern Nepal and Tibet): Record of an Exhumation History. In: Geological Society of London, Special Publication, vol. 74 323–340.
Ray, S., 1947. Zonal metamorphism in the eastern Himalayas and some aspects of local geology. Quarterly Journal of the Geological Mining and Metallurgical Society of India 19, 117–139.
Robinson, D.M., DeCelles, P.G., Patchett, P.J., Garzione, C.N., 2001. The kinematic evolution of the Nepalese Himalaya interpreted from Nd isotopes. Earth and Planetary Science Letters 192, 507–521.
Robinson, D.M., DeCelles, P.G., Copeland, P., 2006. Tectonic evolution of the Himalayan thrust belt in western Nepal: implications for channel flow models. Geological Society of America Bulletin 118, 865–885.
Rowley, D.B., 1996. Age of initial collision between India and Asia: a review of stratigraphic data. Earth and Planetary Science Letters 145, 1–13.
Rutter, E.H., 1976. The Kinetics of Rock Deformation by Pressure Solution. In: Philosophical Transactions Royal Society of London A, vol. 283 203–219.
Rutter, E.H., 1983. Pressure solution in nature, theory and experiment. Journal of Geological Society of London 140, 725–740.
Schmid, S.M., 1975. The Glarus Overthrust: Field Evidence Mechanical Model, 68, pp. 247–280.
Schmid, S.M., 1982. Microfabric studies as indicators of deformation mechanisms and flow laws operative in mountain building. In: Hsu, K.J. (Ed.), Mountain Building Processes. Academic Press, pp. 95–110.
Schwan, W., 1980. Shortening Structures in Eastern and North-western Himalayan Rocks. In: Saklani, P.S. (Ed.). Today and Tomorrow's Printers and Publishers, New Delhi.
Searle, M.P., Law, R.D., Godin, L., Larson, K.P., Streule, M.J., Cottle, J.M., Jessup, M.J., 2008. Defining the Himalayan main central thrust in Nepal. Journal of Geological Society of London 165, 523–534.
Shea Jr., W.T., Kronenberg, A.K., 1993. Strength and anisotropy of foliated rocks with varied mica contents. Journal of Structural Geology 15, 1097–1122.
Sibson, R.H., 1977. Fault rocks and fault mechanisms. Journal of the Geological Society of London 133, 191–213.
Sibson, R.H., White, S.H., Atkinson, B.K., 1981. Structure and distribution of fault rocks in the Alpine fault zone, New Zealand. In: McClay, K.R., Price, N.J. (Eds.), Thrust and Nappe Tectonics. Geological Society of London Special Publication, vol. 9, pp. 197–210.
Sinha-Roy, S., 1982. Himalayan Main Central thrust and its implications for Himalayan inverted metamorphism. Tectonophysics 84, 197–224.
Sorkhabi, R.B., Macfarlane, A., 1999. Himalaya and Tibet: mountain roots to mountain top. In: Macfarlane, A., Sorkhabi, R.B., Quade, J. (Eds.), Himalaya and Tibet: Mountain roots to mountain top: Geological Society of America Special paper 328, 1–7.
Srivastava, P., 1993. Stratigraphy, Deep Structure, and Structural Evolution of the Kumaon and Garhwal Himalaya (India). PhD thesis, University of Rochester, pp. 1–220.
Srivastava, P., Mitra, G., 1994. Thrust geometries and deep structure of the Outer and Lesser Himalaya, Kumaon and Garhwal (India): implications for evolution of the Himalayan fold-and-thrust belt. Tectonics 13, 89–109.
Srivastava, P., Mitra, G., 1996. Deformation mechanisms and inverted thermal profile in the North Almora Thrust mylonite zone, Kumaon Lesser Himalaya, India. Journal of Structural Geology 18, 27–39.
Srivastava, H.B., Tripathy, N.R., 2007. Geometrical analysis of mesoscopic shear zones in the crystalline rocks of MCT zone of Garhwal Higher Himalaya. Journal of Asian Earth Sciences 30, 599–612.
Sussman, A. J., 1995. Geometry, Deformation History and Kinematics in the Footwall of the Canyon Range Thrust, Central Utah. M.Sc. thesis, Universtiy of Rochester. 119.
Tharp, T.M., 1983. Analogies between the high-temperature deformation of polyphase rocks and the mechanical behavior of porous powder material. Tectonophysics 96, T1–T11.
Tullis, J., Yund, R.A., 1980. Hydrolytic weakening of experimentally deformed Westerly granite and Hale albite rock. Journal of Structural Geology 2, 439–451.
Tullis, J., Yund, R.A., 1985. Dynamic recrystallization of feldspar: a mechanism for ductile shear zone formation. Geology 13, 238–241.
Tullis, J., Yund, R.A., 1987. Transition from cataclastic flow to dislocation creep of feldspar: mechanisms and microstructures. Geology 15, 606–609.
Tullis, J., Wenk, H.-R., 1994. Effect of muscovite on the strength of lattice preferred orientations of experimentally deformed quartz aggregates. Materials Science and Engineering A 175, 209–220.
Underwood, E.E., 1970. Quantitative Stereology. Addison-Wesley, Reading, Massachusetts, p. 274.
Valdiya, K.S., 1980. The two intracrustal boundary thrusts of the Himalaya. Tectonophysics 66, 323–348.
Valdiya, K.S., 1980. Geology of Kumaon Lesser Himalaya. Wadia Institute of Himalayan Geology, Dehradun, India.

White, S., 1976. The Effects of Strain on the Microstructures, Fabrics, and Deformation Mechanisms in Quartzites. In: Philosophical Transactions Royal Society of London A, vol. 283 69–86.
White, S., Knipe, R.J., 1978. Transformation- and reaction- enhanced ductility in rocks. Journal of Geological Society of London 135, 513–516.
White, S.H., Burrows, S.E., Carreras, J., Shaw, N.D., Humphreys, F.J., 1980. On mylonites in ductile shear zones. Journal of Structural Geology 2, 175–187.
Wojtal, S., Mitra, G., 1986. Strain hardening and strain softening in fault zones from foreland thrust. Geological Society of America Bulletin 97, 674–687.
Wojtal, S., Mitra, G., 1988. Nature of deformation in fault rocks from Appalachian thrusts. In: Mitra, G., Wojtal, S. (Eds.), Geometry and Mechanisms of Thrusting with Special Reference to the Appalachians. Geological Society of America Special Paper, 222, pp. 17–34.
Yardley, B.W.D., 1989. An introduction to metamorphic petrology. Longman Scientific and Technical Pub., pp. 248